JGR Earth Surface

RESEARCH ARTICLE
10.1029/2021JF006392

A Mechanistic Model for Mud Flocculation in Freshwater Rivers

Justin A. Nghiem[1], Woodward W. Fischer[1], Gen K. Li[1,2], and Michael P. Lamb[1]

[1]Division of Geological and Planetary Sciences, California Institute of Technology, Pasadena, CA, USA, [2]Now at Department of Earth Science, University of California, Santa Barbara, CA, USA

Key Points:

- Turbulence, sediment concentration and mineralogy, water chemistry, and organics affect river floc size and settling velocity
- Controlling variables are incorporated into a model for mud floc diameter and settling velocity in rivers calibrated on a global data set
- Mud flocs in rivers can respond to river hydraulics and biogeochemistry with implications for the carbon cycle and fluvial morphodynamics

Supporting Information:

Supporting Information may be found in the online version of this article.

Correspondence to:

Justin A. Nghiem,
jnghiem@caltech.edu

Citation:

Nghiem, J. A., Fischer, W. W., Li, G. K., & Lamb, M. P. (2022). A mechanistic model for mud flocculation in freshwater rivers. *Journal of Geophysical Research: Earth Surface*, *127*, e2021JF006392. https://doi.org/10.1029/2021JF006392

Received 15 AUG 2021
Accepted 2 APR 2022

Abstract The transport and deposition of mud in rivers are key processes in fluvial geomorphology and biogeochemical cycles. Recent work indicates that flocculation might regulate fluvial mud transport by increasing mud settling velocities, but we lack a calibrated mechanistic model for flocculation in freshwater rivers. Here, we developed and calibrated a semi-empirical model for floc diameter and settling velocity in rivers. We compiled a global data set of river suspended sediment concentration-depth profiles and inverted them for in situ settling velocity using the Rouse-Vanoni equation. On average, clay and silt (diameters <39 μm) are flocculated with settling velocity of 1.8 mm s^{-1} and floc diameter of 130 μm. Among model variables, Kolmogorov microscale has the strongest positive correlation with floc diameter, supporting the idea that turbulent shear limits floc size. Sediment Al/Si (a mineralogy proxy) has the strongest negative correlation with floc diameter and settling velocity, indicating the importance of clay abundance and composition for flocculation. Floc settling velocity increases with greater mud and organic matter concentrations, consistent with flocculation driven by particle collisions and binding by organic matter which is often concentrated in mud. Relative charge density (a salinity proxy) correlates with smaller floc settling velocities, a finding that might reflect the primary particle size distribution and physical hosting of organic matter. The calibrated model explains river floc settling velocity data within a factor of about two. Results highlight that flocculation can impact the fate of mud and particulate organic carbon, holding implications for global biogeochemical cycles.

Plain Language Summary The fate of fine sediment in rivers is important for understanding contaminant dispersal, organic carbon burial, and the construction of river floodplains and deltas. Individual grains of silt and clay dispersed in water settle under the pull of gravity at extremely slow rates. However, in natural rivers, these mud particles can aggregate together into larger structures called flocs, resulting in far faster settling rates. Here, we built on prior work from estuaries to develop a settling velocity model for flocculated mud in freshwater rivers. Our results demonstrate that mud settling velocity increases in rivers with less vigorous turbulence because turbulence can break flocs apart. Mud settling velocity also increases with greater concentrations of mud and particulate organic matter, which promote particle collisions and binding. Counterintuitively, settling velocity decreases with greater clay abundance and greater river water salinity, possibly due to how they affect organic matter in binding mud particles into flocs. Our results improve understanding of floc behavior in rivers and indicate potential links between the routing of mud and organic matter, river geomorphology, and global climate.

1. Introduction

Mud (grain diameter, D < 62.5 μm) dominates the sediment load carried by rivers globally (e.g., Baronas et al., 2020; Lupker et al., 2011) and its fate is important for our understanding of fluvial geomorphology and biogeochemical cycling. For example, mud-rich fluvial deposits are a major component of the rock record (Aller, 1998; McMahon & Davies, 2018; Zeichner et al., 2021). Mud cohesion increases bank strength in alluvial rivers, affecting river morphodynamics (e.g., Dunne & Jerolmack, 2020; Kleinhans et al., 2018; Lapôtre et al., 2019; Millar & Quick, 1998). Mud is also a primary carrier of organic carbon and pollutants because of its high specific surface area (e.g., France-Lanord & Derry, 1997; Galy et al., 2015; Pizzuto et al., 2014). Despite its importance, we lack well-tested mechanistic models for mud transport in rivers.

Mud in rivers has traditionally been treated as washload, or sediment that is too fine to regularly settle to and interact with the riverbed (Church, 2006; Garcia, 2008). In contrast, recent work suggests that flocculation—the aggregation of particles into composite structures called flocs—can enhance mud settling velocities and

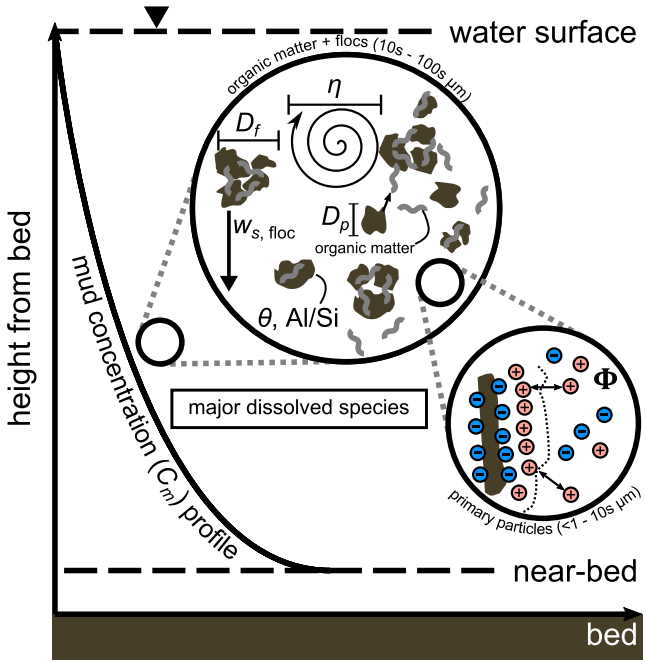

Figure 1. Schematic of a cross-section through a river water column illustrating physicochemical processes operating at different scales that could be important for mud flocculation in rivers. Key variables are turbulence (Kolmogorov microscale, η), volumetric mud concentration (C_m), sediment mineralogy (molar Al/Si of river suspended sediment), organic matter concentration (fraction of sediment surface covered by organic matter, θ), and dissolved species concentrations (relative charge density of river water, Φ). These variables affect the diameter, D_f, and settling velocity, $w_{s,floc}$, of flocs composed of primary particles with diameter D_p.

drastically affect mud transport dynamics in rivers (Bouchez, Métivier, et al., 2011; Lamb et al., 2020; Zeichner et al., 2021). Similar to sand, flocculated mud might be in a dynamic interchange between the flow and bed material (Lamb et al., 2020). Mud flocculation has been well-studied in estuarine and marine systems where flocs form in part because salinity promotes van der Waals attraction between particles (e.g., Hill et al., 2000; Mehta & Partheniades, 1975; Winterwerp, 2002, Figure 1). In addition, flow turbulence, sediment concentration, organic matter concentration, and clay mineralogy are important for estuarine and marine flocculation (e.g., Kranck & Milligan, 1980; Meade, 1972; Verney et al., 2009). In contrast to the wealth of studies on flocculation in saline environments, knowledge on flocculation in freshwater rivers is relatively limited (e.g., Bungartz & Wanner, 2004; Droppo et al., 1997; Droppo & Ongley, 1994).

Studies in rivers identified flow characteristics, organic matter concentration, and suspended sediment concentration as potential controls on floc size, settling velocity, and strength (Figure 1). Through microscopy of samples from Canadian rivers, Droppo and Ongley (1994) observed organic matrices binding together mineral sediment into flocs. They observed correlations between floc size and suspended sediment concentration, attached bacteria count, and particulate organic carbon concentration. Bungartz et al. (2006) characterized floc setting velocities at three transects along a lake outlet and found faster-settling flocs at higher discharge, a result they attributed to faster floc growth at higher flow turbulence. They also showed that settling patterns of suspended sediment and particulate organic carbon were similar, supporting the idea that flocculation controlled transport of both mineral sediment and organic carbon. Gerbersdorf et al. (2008) examined bed material composition in the Neckar River, Germany, and identified rich networks of microbe-derived extracellular polymeric substances (EPS). They found positive correlations between concentrations of EPS moieties and the critical shear stress for erosion, indicating that EPS can help stabilize bed sediment. Lamb et al. (2020) used a field data compilation to infer the presence of widespread mud flocculation in rivers. They showed that in situ particle settling velocity can be inferred by fitting the Rouse-Vanoni equation to grain size-specific suspended sediment concentration-depth profiles. However, they did not explain the order-of-magnitude variation in the inferred floc settling velocities.

Experiments have also supported organic matter, dissolved species, and sediment concentration as important controls on freshwater flocculation (Figure 1). Chase (1979) showed that the presence of organics increased floc settling velocity, a result attributed to the interaction of sediment surface coatings, organic chemistry, and dissolved solutes. Subsequent experiments showed that sediment concentration positively correlated with floc size while fluid shear rate affected floc size and settling velocity differently (e.g., Burban et al., 1990; Tsai et al., 1987). More recent experiments examining the role of organics on flocculation in freshwater highlighted the importance of nutrients, biomass, and organic matter composition on floc size and settling velocity (Furukawa et al., 2014; Lee et al., 2017, 2019; Tang & Maggi, 2016; Zeichner et al., 2021). For instance, Zeichner et al. (2021) showed in experiments modeled after rivers that organic matter increased clay floc settling velocities by up to three orders of magnitude, depending on organic matter type and clay mineralogy.

Process-based flocculation theory is required to link field studies and experiments into a coherent framework. Floc population balance models use particle aggregation and breakage kernels, and have been successful at reproducing floc size distributions (e.g., Lick & Lick, 1988; Spicer & Pratsinis, 1996; Xu et al., 2008). These studies showed that sediment concentration and fluid shear enhance floc aggregation by increasing particle collision frequency, but greater shear causes floc breakage (Figure 1). Winterwerp (1998) introduced a simplified model (hereafter, the Winterwerp model) tracking a characteristic floc diameter (e.g., the median), making it more easily coupled to hydrodynamic models (e.g., Maggi, 2008; Son & Hsu, 2011; Winterwerp, 2002). The Winterwerp model includes the effects of fluid shear and sediment concentration, but subsumes other factors into coefficients

of the aggregation and breakage rates. The model describes well the equilibrium size of flocculated estuarine mud (Winterwerp, 1998) and flocs in saline laboratory experiments (e.g., Kuprenas et al., 2018; Maggi, 2009; Son & Hsu, 2008). However, these models have yet to be compared or adapted to flocculation in freshwater rivers.

Here, we built on the Winterwerp approach to develop a semi-empirical process-based model for mud flocculation in freshwater rivers. First, we proposed new forms for flocculation efficiency coefficients to explicitly cast floc diameter and settling velocity as functions of physicochemical variables that prior work has shown are important for flocculation in freshwater: turbulence, sediment concentration, sediment mineralogy, organic matter concentration, and dissolved ion concentration (Figure 1). Next, we calibrated the new model against field data. We compiled a global data set of river grain size-specific suspended sediment concentration-depth profiles and inverted them for in situ settling velocity using the Rouse-Vanoni equation (Lamb et al., 2020). Together with a river geochemistry data compilation, we fitted the model to help explain the variance in floc settling velocities. Finally, the results are discussed in the context of fluvial geomorphology, organic carbon, tectonics, and climate.

2. Model Development

2.1. Winterwerp Model

Winterwerp (1998) proposed a flocculation model in which fluid shear drives particle collisions and floc aggregation and breakage. The model casts the time rate of change of floc diameter, D_f (or median D_f for a floc size distribution) as the difference of floc aggregation and breakage rates:

$$\frac{\mathrm{d}D_f}{\mathrm{d}t} = \frac{k_A}{n_f \eta^2} \nu C D_f \left(\frac{D_f}{D_p}\right)^{3-n_f} - \frac{k_B}{n_f \eta^2} \nu D_f \left(\frac{D_f - D_p}{D_p}\right)^{3-n_f} \left(\frac{\tau_t}{\tau_y}\right)^{j} \quad (1)$$

On the right-hand side of Equation (1), the first term is the floc aggregation rate, scaled by the aggregation efficiency, k_A (dimensionless), and the second term is the floc breakage rate, scaled by the breakage efficiency, k_B (dimensionless). The shear rate, G (s^{-1}), quantifies fluid mixing and relates to the smallest turbulence length scale— the Kolmogorov microscale, $\eta = \sqrt{\nu/G}$ (m), where ν is the fluid kinematic viscosity ($m^2\ s^{-1}$) (Tennekes & Lumley, 1972). Greater fluid mixing and volumetric sediment concentration, C (volume sediment/total volume; dimensionless), drive more frequent collisions of primary particles with diameter D_p (m) and thereby increase aggregation rate (Figure 1).

Flocs break up if fluid shear is too high relative to floc strength, an effect that Winterwerp (1998) expressed in Equation (1) using the ratio of fluid stress on the floc, $\tau_t = \rho(\nu/\eta)^2$ (Pa), and floc strength, $\tau_y = F_y/D_f^2$ (Pa), where ρ is fluid density ($kg\ m^{-3}$). F_y is floc yield strength (in terms of force) and has been estimated to be of order 10^{-10} N (Matsuo & Unno, 1981). Floc fractal dimension, $n_f \in [1,3]$ (dimensionless), describes floc structure assuming it is approximately self-similar (Kranenburg, 1994). Floc structure can vary from a linear string of particles ($n_f = 1$) to a solid, compact particle ($n_f = 3$). An average $n_f = 2$ is typical for natural flocs (e.g., Tambo & Watanabe, 1979; Winterwerp, 1998). In practice, n_f describes the relationship between floc diameter and floc density by $R_f/R_s = (D_f/D_p)^{n_f-3}$ where R_f is the floc submerged specific gravity (dimensionless) and R_s is the submerged specific gravity of the primary particle sediment (dimensionless) (Kranenburg, 1994). Although the parameter j in Equation (1) is an empirical constant, Winterwerp (1998) used $j = 0.5$ to ensure that floc settling velocity, floc diameter, and sediment concentration are linearly related to each other based on estuarine floc data. We retained j as a fit parameter to maintain generality.

2.2. Modifications to the Winterwerp Model for River Flocs

We proposed changes to floc strength, and floc aggregation and breakage efficiencies to adapt the Winterwerp model to rivers.

2.2.1. Floc Strength

Experiments in freshwater have shown that, for constant D_f, floc settling velocity, $w_{s,\mathrm{floc}}$, increases with larger mixing rate due to an increase in floc density (Burban et al., 1990). This behavior suggests that flow conditions during floc formation can affect floc strength, where more porous and lighter flocs are weaker because they have fewer interparticle contacts and vice versa. Bache (2004) proposed that floc strength, τ_y, is a balance of local

turbulent kinetic energy per unit volume acting on the floc and the energy per unit volume required to rupture the floc:

$$\tau_y = \frac{\rho}{30}\left(\frac{\nu}{\eta}\right)^2\left(\frac{D_f}{\eta}\right)^2 \tag{2}$$

The power-law form of Equation (2) holds in general but the numerical constants apply for small D_f/η (Bache, 2004).

2.2.2. Floc Aggregation and Breakage Efficiencies

In the Winterwerp model, all contributions to flocculation outside of fluid shear and sediment concentration are captured in the constant floc aggregation and breakage efficiency terms, k_A and k_B, respectively. We investigated whether k_A and k_B in rivers depend on organic matter concentration, sediment mineralogy, and dissolved ion concentration, as functions rather than fit constants.

Organic matter can adsorb onto sediment surfaces and form connective "bridges" between grains (Ruehrwein & Ward, 1952; Smellie & La Mer, 1958; Molski, 1989, Figure 1). In rivers, biogenic molecules like EPS can act as sticky media for bridging flocculation (Droppo & Ongley, 1994; Gerbersdorf et al., 2008; Larsen et al., 2009; Lee et al., 2019). Smellie and La Mer (1958) proposed a functional form of bridging flocculation efficiency,

$$k_A,\ k_B^{-1} \propto \theta(1-\theta) \tag{3}$$

in which θ is the fraction of the sediment surface covered by a polymeric substance. We used Equation (3) and calculated θ for organic matter (Section 3.3).

We accounted for sediment mineralogy using the molar elemental ratio Al/Si as a proxy variable (Figure 1). More intensely weathered rocks typically generate sediment with larger Al/Si because chemical weathering produces Al-rich clay minerals (e.g., Ito & Wagai, 2017; Jackson et al., 1948; Lupker et al., 2012). Mineralogy can affect flocculation because it determines the range of potential chemical interactions between particles through cation exchange capacity (CEC) and therefore the ability to attract cations in solution (Mehta & McAnally, 2008). Furthermore, cations can affect the ability of organic matter to adsorb to particle surfaces and the physical orientation of adsorbed organic matter (Galy et al., 2008; Mehta & McAnally, 2008). We used a simple power law model as a starting point,

$$k_A \propto (\mathrm{Al/Si})^{A_1} \tag{4}$$

$$k_B \propto (\mathrm{Al/Si})^{B_1} \tag{5}$$

where A_1 and B_1 are dimensionless fit constants.

Dissolved ions in river water might promote flocculation through the same mechanism as salinity by boosting the effectiveness of van der Waals attraction between particles (e.g., Seiphoori et al., 2021, Figure 1). To express ionic effects, we used a dimensionless parameter, Φ, to quantify the relative densities of charges in solution and on the sediment (Rommelfanger et al., 2020):

$$\Phi = \frac{\lambda I}{\mathrm{CEC}\,\rho_s L/2} \tag{6}$$

in which the Debye length, λ (m), is the average length from the particle in which an electrostatic effect from the charged surface is sustained, I is the solution ionic strength ((number ions) m^{-3}), CEC is the sediment CEC ((number ions) kg^{-1}), ρ_s is sediment density (kg m^{-3}), and L (m) is a grain length scale that is nominally the face length of a plate-shaped clay particle, which we set to D_p. Physically, Φ quantifies the ionic strength of river water relative to the ionic strength in a volume surrounding primary particles. As Φ increases, the positive charge in the water within the Debye length overcomes the negative charge on the sediment surface and causes attraction between nearby sediment grains (Rommelfanger et al., 2020). We proposed power-law relations as starting points to relate Φ and the flocculation efficiencies:

$$k_A \propto \Phi^{A_2} \tag{7}$$

$$k_B \propto \Phi^{B_2} \tag{8}$$

where A_2 and B_2 are dimensionless fit constants.

2.3. River Floc Model

We substituted Equations (2) – (8) into Equation (1) to derive a modified semi-empirical model for floc diameter, D_f:

$$\frac{\mathrm{d}D_f}{\mathrm{d}t} = \frac{k'_A\theta(1-\theta)(\mathrm{Al/Si})^{A_1}\Phi^{A_2}}{n_f\eta^2}\nu C D_f\left(\frac{D_f}{D_p}\right)^{3-n_f} - \frac{k'_B(\mathrm{Al/Si})^{B_1}\Phi^{B_2}}{\theta(1-\theta)n_f\eta^2}\nu D_f\left(\frac{D_f-D_p}{D_p}\right)^{3-n_f}\left(\frac{\eta}{D_f}\right)^{2j} \quad (9)$$

in which k'_A and k'_B are new dimensionless constants that absorb all constant dimensionless parameters related to floc aggregation and breakage, respectively. At dynamic equilibrium, the time derivative of D_f vanishes, resulting in

$$D_f = k\eta\left(C\theta^2(1-\theta)^2\right)^q(\mathrm{Al/Si})^r\Phi^s\left(1-\frac{D_p}{D_f}\right)^{-q(3-n_f)} \quad (10)$$

in which $k = \left(k'_B/k'_A\right)^{1/(2j)}$, $q = -1/(2j)$, $r = (B_1 - A_1)/(2j)$, and $s = (B_2 - A_2)/(2j)$. We consolidated the unknown dimensionless coefficients and variables into the coefficient k and exponents q, r, and s. D_f appears on both sides of Equation (10), so we simplified the equation by assuming that $D_f \gg D_p$:

$$D_f = k\eta\left(C\theta^2(1-\theta)^2\right)^q(\mathrm{Al/Si})^r\Phi^s \quad (11)$$

The assumption $D_f \gg D_p$ makes D_f independent of D_p in Equation (11) and implies a model domain of validity of intermediate fluid shear such that D_f does not converge to D_p. We validated the assumption through analysis of our field data compilation (Section 4.1). The equilibrium D_f model is plausible in rivers because experiments and field studies have shown the time scale for unsteady floc behavior to reach equilibrium in river conditions is typically on the order of tens of minutes to hours, and most dynamic river processes (e.g., floods) have longer time scales (e.g., Bungartz et al., 2006; Garcia-Aragon et al., 2011).

Floc settling velocity, $w_{s,\mathrm{floc}}$, relates to D_f using an adaptation of the Stokes settling law for flocs (Strom & Keyvani, 2011; Winterwerp, 1998) as

$$w_{s,\,floc} = \frac{R_s g D_p^2}{c_1\nu}\left(\frac{D_f}{D_p}\right)^{n_f-1} \quad (12)$$

Substituting Equation (11) into Equation (12) yields a model for $w_{s,\mathrm{floc}}$

$$w_{s,\,floc} = \frac{R_s g D_p}{c_1\nu}\left[k\frac{\eta}{D_p}\left(C\theta^2(1-\theta)^2\right)^q(\mathrm{Al/Si})^r\Phi^s\right]^{n_f-1} \quad (13)$$

Flocs have irregular shapes and variable porosity which complicate the relationship between floc diameter and settling velocity (van Leussen, 1988). In Equation (13), the effects of floc shape and porosity on $w_{s,\mathrm{floc}}$ are captured in the dimensionless parameters c_1 and n_f. We held them constant at $c_1 = 20$ (Strom & Keyvani, 2011; Winterwerp, 1998) and $n_f = 2$ (Kranenburg, 1994; Tambo & Watanabe, 1979). Combining these assumptions with Equation (13) yields

$$w_{s,\,floc} = \frac{R_s g D_p}{20\nu}k\eta\left(C\theta^2(1-\theta)^2\right)^q(\mathrm{Al/Si})^r\Phi^s \quad (14)$$

Equation (14) demonstrates that different c_1 values do not affect model calibration because model fitting absorbs multiplicative constants into the prefactor k. However, different n_f values affect model calibration because Equation (13) depends nonlinearly on n_f, an effect we explored in sensitivity tests (Section 4.2).

3. Field Data Methods

3.1. River Suspended Sediment Concentration-Depth Profiles

We compiled a data set of grain size-specific suspended sediment concentration-depth profiles containing 122 profiles from 12 rivers distributed globally (Table S1 in Supporting Information S1). We targeted datasets with suspended sediment concentration for multiple heights in the water column, laser-diffraction grain size analysis, water depth, and boundary shear velocity data. We used datasets analyzed by de Leeuw et al. (2020) and Lamb et al. (2020), and included additional datasets (Abraham et al., 2017; Baronas et al., 2020; Bouchez, 2022; Bouchez, Lupker et al., 2011, 2012; Dingle, 2021; Dingle et al., 2020) (Table S1 in Supporting Infomation S1).

Having a detailed grain size distribution for each suspended sediment sample is vital because it permits the construction of concentration-depth profiles for every grain size class (denoted i). We refer to these profiles as grain size-specific concentration-depth profiles. In other words, a single profile of suspended sediment samples yields as many grain size-specific concentration-depth profiles as there are measured grain size classes. We took advantage of grain size data to fit the Rouse-Vanoni equation and invert for in situ settling velocity as a function of the measured grain size (Figure 1). The measured grain sizes are those of unflocculated sediment (i.e., the primary particles) because size distribution measurements were made after dispersing the sediment (e.g., Baronas et al., 2020).

The Rouse-Vanoni equation is

$$C_i(z) = C_{bi}\left(\frac{\frac{h-z}{z}}{\frac{h-h_b}{h_b}}\right)^{p_i} \tag{15}$$

in which the volumetric sediment concentration for the ith grain size class, C_i, is a function of height from the bed, z, water depth, h, and a near-bed concentration, C_{bi}, specified at a near-bed height, $z = h_b$ (Rouse, 1937). The Rouse number (dimensionless) is $p_i = w_{si}/(\beta_i \kappa u_*)$ in which $\kappa = 0.41$ is the von Kármán constant (dimensionless), u_* (m s^{-1}) is the boundary shear velocity, w_s (m s^{-1}) is the sediment settling velocity, and β is the ratio of sediment and fluid diffusivities (Rouse, 1937) where i indexes the grain size class. Following de Leeuw et al. (2020) and Lamb et al. (2020), we fitted Equation (15) to the compiled grain size-specific concentration-depth profiles to estimate C_b and p for each grain size class. We estimated p_i and C_{bi} (at $z = h_b = 0.1\ h$) from fitting the log-transformed Equation (15) using ordinary least squares regression. We computed the 68% confidence intervals on the fitted p_i from the regression and discarded profiles in which the lower confidence bound on p_i is negative because these profiles do not follow Rouse-Vanoni theory for unknown reasons (e.g., non-equilibrium sediment transport, sampling and/or measurement errors).

We needed to specify u_* and β_i to estimate the grain size-specific in situ settling velocity, w_{si}, from the fitted value of p_i. We used u_* reported in the original data sources, which were measured concurrently with suspended sediment samples and typically calculated by fitting flow velocity profiles measured using an acoustic Doppler current profiler to the law of the wall (e.g., Wilcock, 1996). β is a major unknown in calculating settling velocities from fitted Rouse numbers (e.g., de Leeuw et al., 2020). Empirically, β is commonly found to increase with w_s/u_* (de Leeuw et al., 2020; Graf & Cellino, 2002; Santini et al., 2019; van Rijn, 1984). $\beta < 1$ corresponds to greater sediment concentration stratification compared to $\beta = 1$, which could result from turbulence damping due to suspended sediment-induced density stratification (Graf & Cellino, 2002; Wright & Parker, 2004; discussion in de Leeuw et al., 2020). The reasons for $\beta > 1$ are less clear, but might be linked to enhanced mixing from bedform-generated turbulence (Graf & Cellino, 2002) or the high vertical concentration gradient of fast-settling particles promoting sediment diffusion relative to eddy diffusion (Smith & McLean, 1977).

We followed de Leeuw et al. (2020) and empirically fitted functions for β_i using only suspended sand because we assumed sand was unflocculated and settled in situ at theoretical settling velocities. To calculate theoretical sand settling velocities, we used the Ferguson and Church (2004) model (that is, $w_s = \left(R_s g D^2\right)/\left(c_{1,sand}\nu + \sqrt{0.75 c_{2,sand} R_s g D^3}\right)$ with $c_{1,\mathrm{sand}} = 20$ and $c_{2,\mathrm{sand}} = 1.1$), which follows Stokes law for small particles and accounts for inertial affects for large particles. We calculated β_i using these theoretical sand settling velocities, u_*, and the fitted p_i. We found values of β_i and w_{si}/u_* that agree with previously proposed relations for $\beta(w_s/u_*)$ (Figure 2). Next, we calibrated the power-law equation $\beta \propto (w_s/u_*)^l$ on the sand

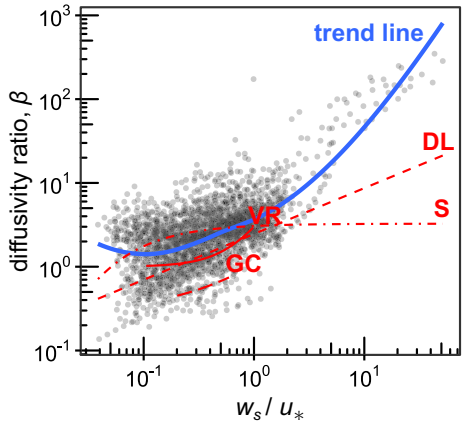

Figure 2. Sediment-fluid diffusivity ratio, β, as a function of settling velocity-shear velocity ratio, w_s/u_*, for sand (diameter, $D > 62.5$ μm) in our concentration-depth profile compilation. Trend line was computed using local polynomial regression. Function abbreviations are VR: van Rijn (1984); GC: Graf and Cellino (2002), their model without bedforms and using a constant median ratio of water depth and bed grain size; S: Santini et al. (2019); DL: de Leeuw et al. (2020), their best-fit one-parameter model for Rouse number.

data within each concentration-depth profile, resulting in a fitted equation for each concentration-depth profile. The median coefficient of determination of the fits is 0.88, indicating a good fit. We assumed that the profile-specific functions $\beta_i = \beta(w_{si}/u_*)$, calibrated on the sand data, were valid for the mud data and extrapolated the fitted β_i functions to calculate w_{si} for the mud size classes (Lamb et al., 2020). We did not explicitly account for the potential effect of hindered settling because 93% of concentration-depth profiles analyzed had mud concentration <5% solids by volume for which hindered settling and density-induced stratification are not expected to be important (Gratiot et al., 2005). However, if hindered settling affected the data, it is implicitly included in our fit values of β_i.

3.2. Extracting River Floc Data

We inferred floc settling velocity, $w_{s,\mathrm{floc}}$, by examining the relationship of particle diameter, D, and the in situ settling velocity, w_s, calculated from fitting the Rouse-Vanoni equation to the concentration-depth profile data. We found good agreement between the Rouse-estimated and predicted settling velocities for sand, but a continuous transition to a settling velocity plateau larger than the theoretical predictions for coarse silt and clay (Figure 3). We attributed the elevated settling velocity of coarse silt and clay to flocculation (Lamb et al., 2020). We found a best-fit two-part piecewise function to quantitatively describe these two settling regimes for each concentration-depth profile (Figure 3; see Text S1 in Supporting Information S1 for details on the fitting method). We termed the diameter at the regime transition the *floc cutoff diameter*, D_t, and interpreted all sediment finer than D_t to be flocculated with a constant $w_{s,\mathrm{floc}}$ for each concentration-depth profile (Lamb et al., 2020, Figure 3).

Next, we computed the floc settling velocity, $w_{s,\mathrm{floc}}$, and primary particle diameter, D_p, from the flocculated data ($D < D_t$). We computed $w_{s,\mathrm{floc}}$ as the mean in situ settling velocities for $D < D_t$ (Figure 3). This method is oversimplified because it implies that all sediment in a given size class for $D < D_t$ was flocculated and settling at the same rate. In reality, some sediment might not have been flocculated and there was likely a distribution of floc sizes and settling velocities in situ (Osborn et al., 2020, 2021), but these distributions cannot be constrained by our data. We also cannot constrain floc structure and the size distribution of the primary particles in individual flocs (e.g., a floc composed of mostly clay might have the same settling velocity as a smaller floc composed of coarse silt with finer sediment bound to its surface). D_p might vary with depth, so we calculated D_p as the median grain size for $D < D_t$ using the depth-averaged concentration of each grain size class as relative weights (Figure 3). We propagated uncertainty to find the 68% confidence intervals for $w_{s,\mathrm{floc}}$ and D_t (Figure 3; Text S1 in Supporting Information S1). Some profiles had data gaps because of the data quality filtering (Section 3.1). We discarded concentration-depth profiles in which D_t was in a data gap greater than one order of magnitude in D. 96 concentration-depth profiles, or about 79% of the initial profiles, remained after this filtering.

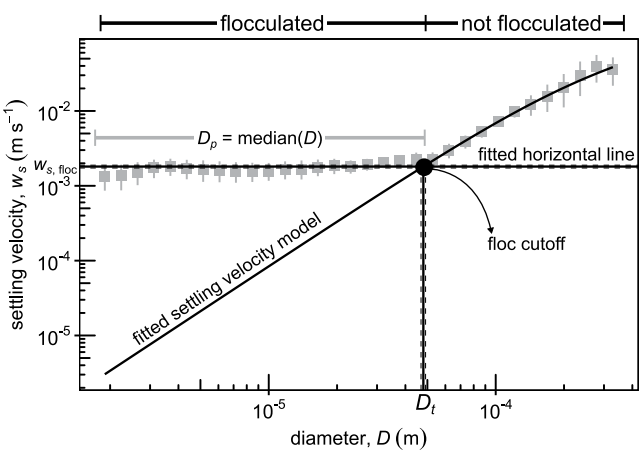

Figure 3. Example of the fitting procedure to estimate floc cutoff diameter, D_t, floc settling velocity, $w_{s,\mathrm{floc}}$, and primary particle diameter, D_p, for a single concentration-depth profile. Each data point represents a single grain size-specific concentration-depth profile. Error bars represent 68% confidence intervals of the linear regression fit to Equation (15). The dashed lines indicate the 68% confidence intervals for $w_{s,\mathrm{floc}}$ and D_t.

We estimated floc diameter, D_f, from the floc cutoff diameter, D_t. D_t, can be interpreted as the diameter of unflocculated grains that settle at the same rate as flocs (Figure 3). Therefore, Stokes law for unflocculated particles applied to D_t results in

$$w_{s,\,floc} = \frac{R_s g D_t^2}{c_1 \nu} \tag{16}$$

combining Equations (12) and (16), we found

$$D_f = D_p\left(\frac{D_t}{D_p}\right)^{\frac{2}{n_f-1}} \tag{17}$$

We used Equation (17) with $n_f = 2$ to calculate D_f. We then combined Equations (11) and (17) to derive a model for D_t:

$$D_t = k(\eta D_p)^{1/2}\left(C\theta^2(1-\theta)^2\right)^q(\mathrm{Al/Si})^r\Phi^s \tag{18}$$

3.3. Estimating Other Variables

We used the depth-averaged volumetric mud concentration, C_m, as the representative sediment concentration in the model (Equations 11, 14 and 18) because we expect flocculation to mainly occur within mud. We found the model goodness-of-fit to be insensitive to the choice of total or mud concentration because they are correlated. We chose typical values for river water density, $\rho = 1000$ kg m^{-3}, sediment density, $\rho_s = 2650$ kg m^{-3}, and kinematic viscosity of water, $\nu = 10^{-6}$ m^2 s^{-1}. We calculated the Kolmogorov microscale using $\eta = \left[\left(\kappa h z \nu^3\right)/\left(u_*^3(h-z)\right)\right]^{1/4}$ for open-channel flow (Nezu & Nakagawa, 1993). The near-bed (at $z = h_b = 0.1\,h$) and depth-averaged η did not vary significantly from each other (within a factor of about 2), so we used the near-bed η in our calculations.

Most data sources for the concentration-depth profiles do not have the requisite geochemical measurements to evaluate the floc model. To supplement, we compiled river geochemistry data from other sources for the same rivers (Table S2 in Supporting Information S1). We matched geochemical measurements to each profile by finding the closest measurements in terms of geographic distance and time of year, weighted equally. The median deviations of the concentration-depth profiles and matched geochemical measurements in time and space are about 4 days and 22 km (or about 54 channel widths). Although these sources of error are difficult to quantify, they should be considered together with the results.

Al/Si is commonly measured for suspended sediment samples, but almost all Al/Si values are measured in bulk without grain size distinction. We compiled and used bulk suspended sediment Al/Si measurements for fitting the model.

We compiled measurements of percent weight organic carbon of suspended sediment samples to estimate θ, the average fraction of sediment covered by organic matter. We assumed cellulose organic matter composition (molar ratio C:H:O of 6:10:5) because it is the most abundant organic compound in the terrestrial biosphere (e.g., Brigham, 2018). We converted measured percent weight organic carbon into percent weight organic matter as cellulose, %OM, using molar mass ratios. Although organic matter usually adsorbs onto sediment in irregular patches (e.g., Ransom et al., 1997), we assumed for simplicity that the volume of organic matter, V_{OM}, is hosted uniformly on the surface of spherical grains with diameter D_p in a shell with volume V_{shell} and thickness δ. With these assumptions, we obtained

$$\theta = \frac{V_{OM}}{V_{shell}} = \frac{(\%OM/100)\frac{\rho_s}{\rho_{OM}}D_p^3}{(D_p+\delta)^3 - D_p^3} \tag{19}$$

We assumed neutrally buoyant organic matter, $\rho_{\mathrm{OM}} = 1000$ kg m^{-3}, and $\delta = 10^{-6}$ m (Barber et al., 2017; Hackley et al., 2017). Measurements of θ for river suspended sediment are unavailable, so we chose δ to obtain θ consistent with $\theta \sim 0.15$ for marine sediment (Bock & Mayer, 2000; Mayer, 1999).

To estimate relative charge density, Φ, we compiled major ion concentrations in rivers (cations: Na^+, K^+, Ca^{2+}, Mg^{2+}; anions: HCO_3^-, SO_4^{2-}, Cl^-). We calculated the molar ionic strength, I, using dissolved ion concentration measurements as $I = 0.5\sum_i c_i z_i^2$ in which c_i is the molar concentration of the ith ion and z_i is its charge number. The Debye length, λ, is expressed as:

$$\lambda = \left(\frac{\epsilon_0\epsilon_r k_{BM} T}{2e^2 z_{\mathrm{cation}}^2 s_{\mathrm{cation}}}\right)^{1/2} \tag{20}$$

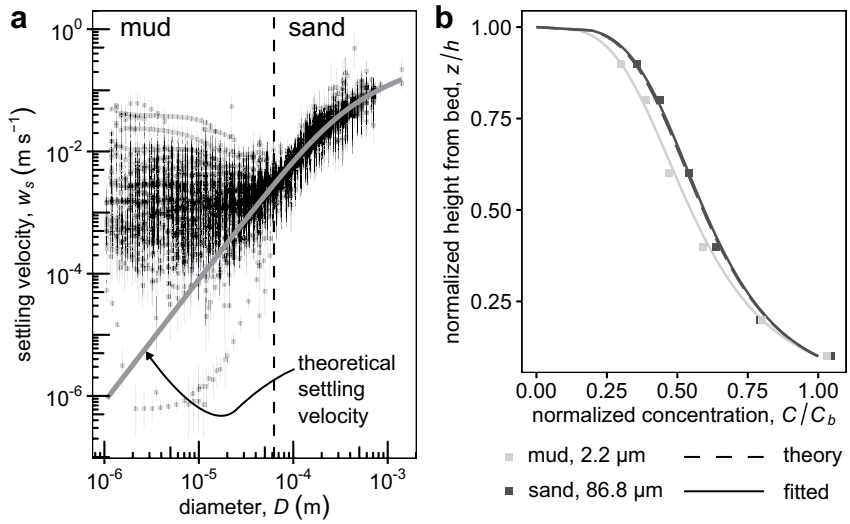

Figure 4. (a) Settling velocity as a function of particle diameter using the Rouse-Vanoni equation method for all compiled suspended sediment concentration-depth profiles. Each data point represents a single grain size-specific concentration-depth profile. Ferguson and Church (2004) shows theoretical settling velocity for unflocculated particles, and follows Stokes law for small particles ($D < \sim 10^{-4}$ m). Error bars represent 68% confidence intervals of the linear regression fit to Equation (15). (b) Example suspended sediment concentration-depth profiles (Moodie et al., 2020) with fitted Rouse-Vanoni equation curves. The dashed lines about each curve mark the 68% confidence interval range.

λ is a function of vacuum permittivity, ϵ_0 (=8.854 × 10^{-12} F m^{-1}), dielectric constant of water, ϵ_r (dimensionless), Boltzmann constant, k_{BM} (=1.381 J K^{-1}), water temperature, T (°C), elementary charge magnitude, e (=1.602 × 10^{-19} C), cation charge number, z_{cation}, and cation concentration, s_{cation} (Rommelfanger et al., 2020). We assumed T = 15°C if it was not reported. We used a temperature-dependent formula to compute ϵ_r (Owen et al., 1961). We calculated z_{cation} from the reported cation concentrations and summed them to obtain s_{cation}. Due to data gaps, we estimated sediment CEC (mol kg^{-1}) from the percent clay of the depth-averaged concentration for each profile using (Ersahin et al., 2006)

$$\mathrm{CEC} = 4.97 + 0.53\,\%\mathrm{clay} \tag{21}$$

in which %clay is the percentage by weight of the total suspended sediment concentration with particle diameters smaller than 2 μm. Equation (21) assumes grain size is a suitable mineralogy proxy to compute CEC.

4. Results

4.1. Floc and Physicochemical Parameters

Results for mud demonstrate an orders-of-magnitude departure of in situ settling velocities, inferred from concentration-depth profile fitting, from predicted settling velocities of unflocculated mud (Figure 4a). Physically, faster mud settling velocity causes a more stratified suspended mud concentration-depth profile (Figure 4b). For example, the Rouse-Vanoni equation predicts particles with D_p = 2 μm should be nearly uniformly mixed in the water column. However, the data show similar stratification between mud and sand profiles (Figure 4b). We interpreted elevated mud settling velocities as a signature of mud flocculation (Lamb et al., 2020).

We estimated the floc cutoff diameter, D_t, primary particle diameter, D_p, floc diameter, D_f, and floc settling velocity, $w_{s,floc}$, for each concentration-depth profile using our piecewise function fits in D-w_s space (summarized in Table 1). The medians indicate that suspended sediment in rivers with diameter smaller than D_t = 39 μm (half the interquartile range, IQR/2 = 22 μm) is flocculated into aggregates with diameter D_f = 130 μm (IQR/2 = 100 μm), settling rates of $w_{s,floc}$ = 1.8 mm s^{-1} (IQR/2 = 1.7 mm s^{-1}), and primary particle diameter of D_p = 12 μm (IQR/2 = 4.5 μm). The estimated $w_{s,floc}$ and D_f indicate a median floc density of ρ_{floc} = 1100 kg m^{-3} (IQR/2 = 160 kg m^{-3}) using Equation (12). As expected, the ρ_{floc} estimates are much smaller than the mineral sediment density (ρ_s = 2650 kg m^{-3}) because flocs contain lighter organic matter and pores. We found

Table 1
Median Values of Parameters Estimated From Our Data Compilation

Variable	Median	IQR/2
Floc cutoff diameter, D_t (μm)	39	22
Floc settling velocity, $w_{s,\mathrm{floc}}$ (mm s^{-1})	1.8	1.7
Floc diameter, D_f (μm)	130	100
Primary particle diameter, D_p (μm)	12	4.5
Floc density, ρ_{floc} (kg m^{-3})	1100	160
Kolmogorov microscale, η (μm)	170	26
Depth-averaged mud volumetric concentration, C_m	1.8×10^{-3}	4.7×10^{-3}
Fraction of sediment surface covered by organic matter, θ	0.070	0.039
Suspended sediment Al/Si [molar ratio]	0.23	0.081
Relative charge density, Φ	2.9×10^{-8}	3.4×10^{-8}

Note. We used half the interquartile range (IQR/2) as a robust measure of spread.

$D_p/D_f = 0.097$ (IQR/2 = 0.057), resulting in a negligible difference between Equations (10) and (11) and justifying the assumption of $D_f \gg D_p$ in the model derivation (Figure 5).

Our finding of $D_t = 39$ μm is similar to the finding of $D_t = 40$ μm by Lamb et al. (2020) even though they used a different method to calculate β_i. Tests with different β_i formulations also demonstrate limited effect on w_{si} and yield the same general pattern of in situ settling velocity versus particle diameter (Text S2; Figure S1 in Supporting Information S1). Although in situ river floc data are rare, Osborn et al. (2020) deployed an in situ camera in the Mississippi river and observed flocs with D_f of 70–130 μm, a range also consistent with our D_f estimates.

The Kolmogorov microscale, η, has been proposed as an upper bound on floc diameter, D_f, because flocs can be efficiently broken by turbulence once they grow to the size of the smallest eddies (e.g., Kuprenas et al., 2018; Tambo & Hozumi, 1979; van Leussen, 1988). We found a narrow range of η in our compilation with a typical value of 200 μm (Figure 6a). D_f estimates are typically of the same scale or smaller than η, indicating that η might limit D_f (Figure 5). However, the data suggest that floc size is not strictly turbulence-limited and can increase beyond η (36% of the data), perhaps due to other physicochemical factors that can be explained by the model (see discussion in Section 4.3) and/or uncertainties in calculating D_f (Equation 17; Section 4.2). Conversely, the cases in which D_f is smaller than η motivate examining effects of sediment concentration and mineralogy, organic matter, and water chemistry on flocculation (Section 4.2).

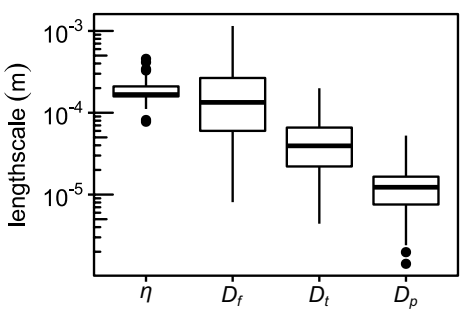

Figure 5. Boxplots of length scales: Kolmogorov microscale, η, floc diameter, D_f, floc cutoff diameter, D_t, and primary particle diameter, D_p, from the data compilation. The lower and upper sides of the boxes indicate the 25th and 75th percentiles, respectively. The whiskers extend 1.5 times the interquartile range below and above the lower and upper sides, respectively. Data beyond the whiskers plot as outlying points.

4.2. Floc Model Calibration

We used sediment Al/Si, depth-averaged volumetric mud concentration, C_m, fraction of sediment surface covered by organic matter, θ, relative charge density, Φ, and primary particle diameter, D_p as independent variables to calibrate the model (Figure 6). Sediment Al/Si ranges from 0.2 to 0.5 (molar ratio) and generally increases with river drainage area (Figure 6b)—a pattern that could reflect production of more Al-rich clay minerals with progressive silicate weathering downstream (e.g., Lupker et al., 2012; West et al., 2005). Depth-averaged volumetric mud concentration, C_m, varies widely across rivers on the order of 10^{-5} to 10^{-2}, a range that likely reflects regional variation in catchment lithology, sediment supply, and transport capacity (Figure 6c). The fraction of sediment surface covered by organic matter, θ, is typically close to 0.1 (Figure 6d). The relative charge density, Φ, largely varies between 10^{-8} and 10^{-7} for our data compilation (Figure 6e) and is a function of weathering contributions to river water ion concentration and electrostatic properties of sediment. Primary particle diameter, D_p, generally

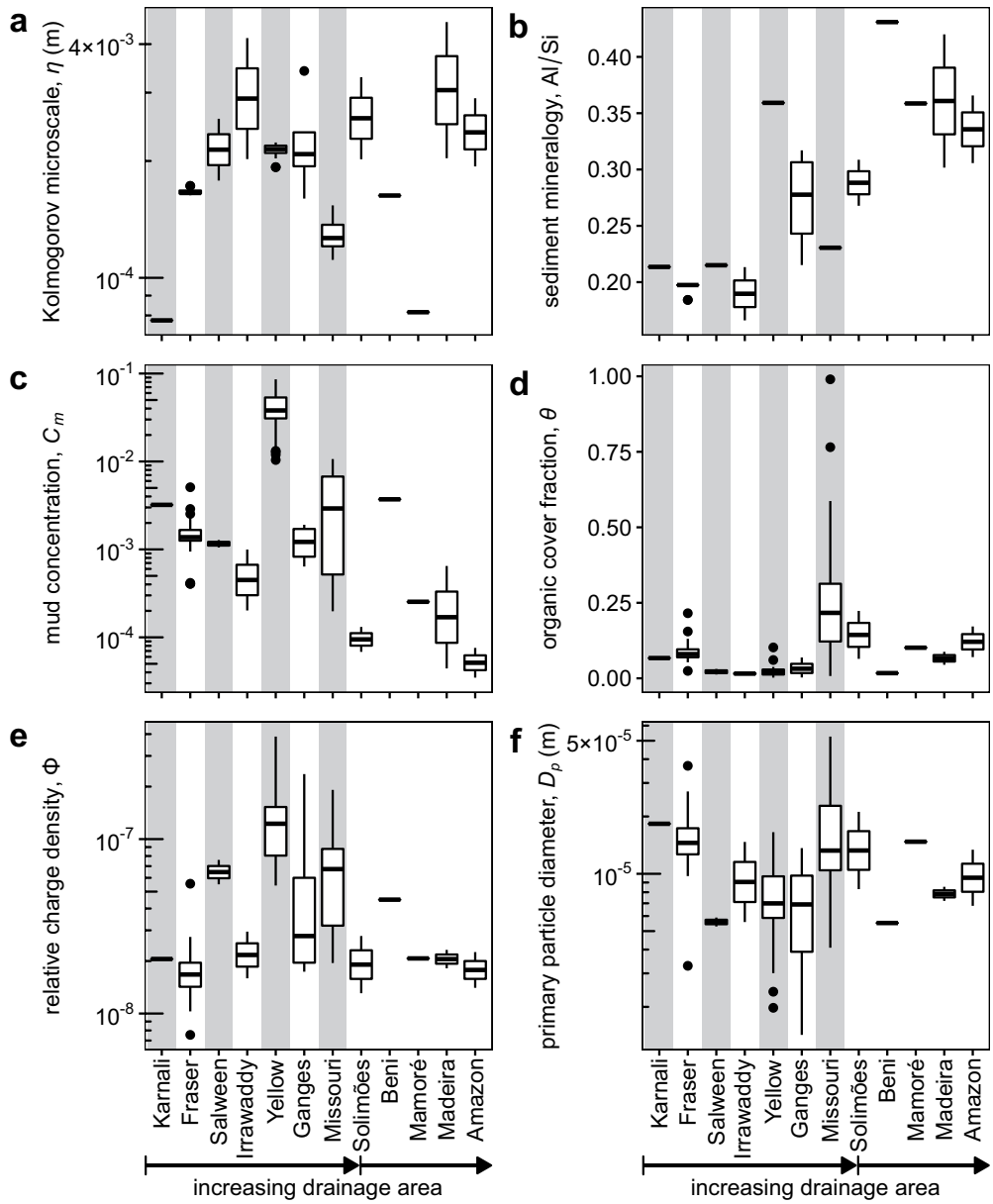

Figure 6. Boxplots of model input variables classified by river. Boxplots that appear as a horizontal line segment contain only a single data point. River names are ordered by increasing drainage area at the sample collection point, measured using HydroSHEDS digital elevation data (Lehner et al., 2008). Amazon Basin Rivers are plotted separately in order of increasing drainage area.

decreases with drainage area (Figure 6f), consistent with downstream grain size fining due to sorting and abrasion (Paola et al., 1992).

We fitted the floc diameter, settling velocity, and cutoff diameter models (Equations 11, 14, and 18) to our D_f, $w_{s,\mathrm{floc}}$, and D_t estimates, respectively (Figure 7; Table 2). The calibrated models with best-fit parameters are:

$$D_t = 0.0187(\eta D_p)^{1/2}\left(C_m\theta^2(1-\theta)^2\right)^{0.0709}(\mathrm{Al/Si})^{-0.792}\Phi^{-0.211} \tag{22}$$

$$w_{s,\,\mathrm{floc}} = \frac{R_s g D_p}{20\nu}0.0284\eta\left(C_m\theta^2(1-\theta)^2\right)^{0.162}(\mathrm{Al/Si})^{-2.22}\Phi^{-0.133} \tag{23}$$

$$D_f = 3.50\times10^{-4}\eta\left(C_m\theta^2(1-\theta)^2\right)^{0.142}(\mathrm{Al/Si})^{-1.58}\Phi^{-0.422} \tag{24}$$

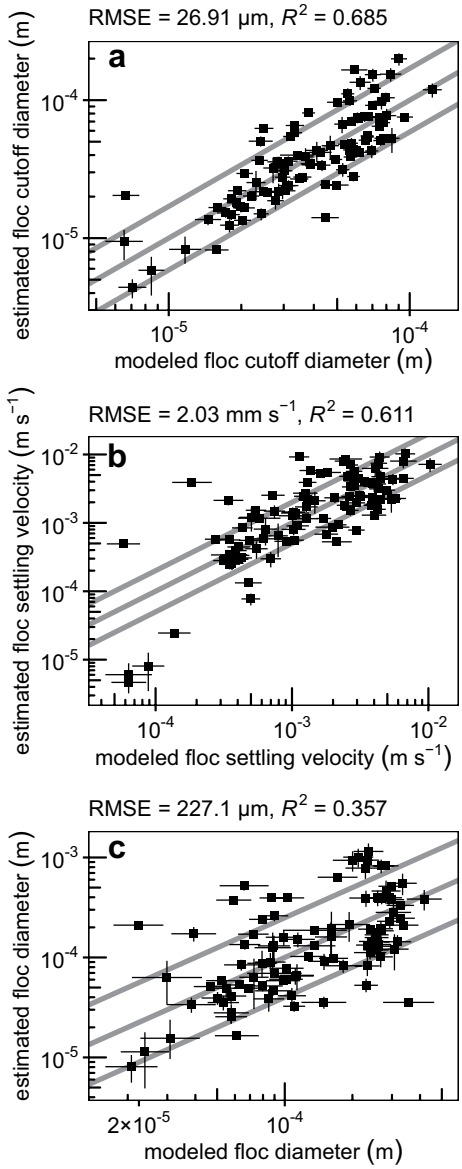

Figure 7. Comparison of the calibrated model for floc cutoff diameter, D_t (panel a), floc settling velocity, $w_{s,\mathrm{floc}}$ (panel b), and floc diameter, D_f (panel c). The central line is 1:1, and the bounding lines indicate the average factor of 1.7, 2, and 2.5 deviation of model values from the data for D_t, $w_{s,\mathrm{floc}}$, and D_f, respectively. Vertical error bars represent the propagated 68% confidence interval. Horizontal error bars represent the standard error range of modeled values.

The majority of the profiles in our compilation was sampled in lowland alluvial rivers, so application of the calibrated model is most appropriate for those settings. The high model goodness-of-fit supports the equilibrium floc assumption in the model (Figure 7; Table 2).

Although the three models are dependent, we fitted the regressions independently of each other because the D_t, $w_{s,\mathrm{floc}}$, and D_f models each include different assumptions. The D_t model is the most direct evaluation of the proposed model parameters because we directly estimated D_t from the concentration-depth profiles (Figure 3) and it is independent of c_1 (Equations 17 and 18), yielding the highest goodness-of-fit among the models (coefficient of determination, $R^2 = 0.685$; root mean square error, RMSE = 26.91 μm). We assumed $n_f = 2$ to derive the D_t model (Equation 17), but model calibrations with different choices of constant n_f show that n_f has a negligible effect on overall goodness-of-fit and minimal effect on calibrated model exponents (Text S3; Figure S2 in Supporting Information S1). Similar to D_t, we estimated $w_{s,\mathrm{floc}}$ directly (Figure 3) and assumed $n_f = 2$ to derive the model (Equation 14). But, in addition, we assumed a constant $c_1 = 20$ (Ferguson & Church, 2004; Strom & Keyvani, 2011) to derive the $w_{s,\mathrm{floc}}$ model (Equation 14), leading to a reduction in the goodness-of-fit ($R^2 = 0.611$; RMSE = 2.03 mm s^{-1}) compared to the D_t model. In contrast to the direct D_t and $w_{s,\mathrm{floc}}$ estimates, D_f was calculated from $w_{s,\mathrm{floc}}$ or D_t. We assumed $n_f = 2$ to calculate D_f from D_t (Equation 17), causing a relatively large drop in goodness-of-fit ($R^2 = 0.357$; RMSE = 227.1 μm) relative to both the D_t and $w_{s,\mathrm{floc}}$ models despite the fact that the D_f model is independent of c_1 and n_f (Equation 11). The differences in goodness-of-fit between the three models indicate the importance of constraining c_1 and n_f, which depend on floc shape and structure (Maggi et al., 2007; Strom & Keyvani, 2011). We calculated the ratio of model predictions and data and took quantiles at 16%, 50% (median), and 84% to characterize the deviation of predictions from the data. We computed quantiles of this ratio at {0.60 (16%), 1.1 (50%), and 1.5 (84%)} for D_t, {0.48, 1.0, and 2.3} for $w_{s,\mathrm{floc}}$, and {0.36, 1.2, and 2.1} for D_f. These results show that the model explains the data within factors of about 1.7 for D_t, 2 for $w_{s,\mathrm{floc}}$, and 2.5 for D_f (Figure 7).

All model exponents (q, r, and s) are significantly different than 0 according to the 95% confidence interval (0.05 significance level) except for the exponent of Φ in the $w_{s,\mathrm{floc}}$ model (Table 2). The reason for the statistical insignificance of Φ in the $w_{s,\mathrm{floc}}$ model is unclear, but might be related to errors in assuming constant c_1 or in matching geochemical measurements to the concentration-depth profiles. The statistical significance of the remaining parameters supports the hypothesis that organic matter, sediment concentration and mineralogy, water chemistry, and turbulence are important predictors of floc properties in rivers.

4.3. Floc Model Dependencies and Interpretation

To isolate the effect of individual parameters on floc settling velocity, we plotted each parameter against the $w_{s,\mathrm{floc}}$ data normalized by all other model terms (Figure 8). We also divided by the median for each normalized quantity to provide comparable scales. The gross trends between individual parameters and $w_{s,\mathrm{floc}}$ are similar to those for D_t and D_f (Figures S3 and S4 in Supporting Information S1).

The Kolmogorov microscale, η, expresses the effect of turbulence on flocs and is predicted to have a positive linear relationship with $w_{s,\mathrm{floc}}$ and D_f (Figure 8a; Figure S4a in Supporting Information S1; Winterwerp, 1998). We tested the plausibility of the relationship between (normalized) $w_{s,\mathrm{floc}}$ and η (e.g., the trend in Figure 8a) using

Table 2
Fitted Parameters in the Floc Model

	Floc cutoff diameter model (Equation 18) $D_t = k(\eta D_p)^{1/2}\left(C_m\theta^2(1-\theta)^2\right)^q(\mathrm{Al/Si})^r\Phi^s$	Floc settling velocity model (Equation 14) $w_{s,floc} = \frac{R_s g D_p}{20\nu}k\eta\left(C_m\theta^2(1-\theta)^2\right)^q(\mathrm{Al/Si})^r\Phi^s$	Floc diameter model (Equation 11) $D_f = k\eta\left(C_m\theta^2(1-\theta)^2\right)^q(\mathrm{Al/Si})^r\Phi^s$
k	0.0187 (0.00307, 0.114)	0.0284 (5.43 × 10^{-4}, 1.49)	3.50 × 10^{-4} (9.45 × 10^{-6}, 0.0129)
q	0.0709 ± 0.0413	0.162 ± 0.0905	0.142 ± 0.0825
r	−0.792 ± 0.418	−2.22 ± 0.916	−1.58 ± 0.836
s	−0.211 ± 0.115	−0.133 ± 0.253	−0.422 ± 0.231

Note. The uncertainties indicate the 95% confidence intervals from an ordinary least squares regression fit. The values in parentheses indicate the lower and upper confidence intervals for k because the interval is asymmetrical.

regression F-tests of the linear relation and an alternative power-law relation. We found a statistically significant linear relationship between normalized $w_{s,\mathrm{floc}}$ and η (p-value = 7.8×10^{-10}) and a statistically insignificant power-law relationship (p-value = 0.33). The linearity between D_f and η agrees with the steady-state equilibrium form of the Winterwerp model (Kuprenas et al., 2018; Winterwerp, 1998).

Mud concentration, C_m, displays a positive sublinear trend with $w_{s,\mathrm{floc}}$ (exponent = 0.162 ± 0.0905; Figure 8b) in contrast to the linear trend predicted by the equilibrium model of Winterwerp (1998). The equilibrium Winterwerp model predicts a linear trend between sediment concentration and floc settling velocity because greater sediment concentration results in proportionally greater interparticle collisions. However, there is a different scaling relation in our model because we allowed the exponent j, which controls the importance of floc strength on the floc breakup rate, to vary (Equations 10 and 11). Inspecting Equation (11), linearity between C_m and $w_{s,\mathrm{floc}}$ occurs only when $j = -0.5$, or $D_f \propto (\tau_y/\tau_t)^{0.5}$, while our calibration indicates that $j = -3.09$, or $D_f \propto (\tau_y/\tau_t)^{3.09}$, which in turn reveals $(\tau_y/\tau_t)^{3.09} \propto (D_f/\eta)^{-2j=2\times3.09=6.18}$. Thus, our calibrated model indicates that the floc breakage rate becomes very large when $D_f > \eta$—much more so than in the Winterwerp model. This finding is consistent with the limiting effect of η on floc size proposed by Kuprenas et al. (2018). But in contrast to their work, our model does not feature a built-in turbulence limit. Rather, D_f can exceed η, but the rapid breakage rates for large flocs make $D_f >> \eta$ less likely. In our equilibrium model, the strong dependence of D_f on η effectively reduces the strengths of dependency on the other input variables. In the case of C_m, fluid shear stresses inhibit the efficiency of sediment concentration to drive floc growth. Thus, although the aggregation rate still depends linearly on C_m in our model, we found a sublinear dependence on C_m for floc diameter and settling velocity.

Organic matter affects flocculation through the fractional cover of organic matter on the surface of sediment grains, θ, according to the function $(\theta^2\ (1\text{-}\ \theta)^2)^q$ with an exponent, $q = 0.162 \pm 0.0905$, identical to that of C_m (Figure 8c). The shared exponent, q, indicates an analogous interpretation: turbulence can promote floc breakage and disrupt the ability of organic matter to facilitate bonding between particle surfaces. Most data display $\theta < 0.5$, a regime in which the function $\theta\ (1\text{-}\ \theta)$ increases with θ. In this domain, the model predicts that increased loading of organic matter promotes larger $w_{s,\mathrm{floc}}$ because the areas of bare sediment and organic matter become more comparable for binding. The positive sublinear exponent implies that increasing organic matter coverage on sediment causes a much larger enhancement of floc size at low θ compared to high θ (but still less than 0.5). Thus, the addition of even small amounts of organic matter to an organics-poor system can trigger an appreciable flocculation response, consistent with experiment results (Zeichner et al., 2021). The model predicts a reverse effect for organics-rich systems, but the sparsity of data for $\theta > 0.5$ precludes confirmation of this behavior.

Sediment Al/Si shows a decreasing trend with $w_{s,\mathrm{floc}}$ (exponent $r = -2.22 \pm 0.916$; Figure 8d). The negative relationship with Al/Si is surprising because Al/Si is typically treated as a clay abundance proxy and clay is expected to be the grain size fraction most susceptible to flocculation (e.g., Mehta & Partheniades, 1975; Van Leussen, 1988). Equation (10) shows that $r = (B_1 - A_1)/(2j)$ where A_1 and B_1 are the respective power-law aggregation and breakage exponents (Equations 4 and 5). We found $j = -3.09$, $r = -2.22$, and hence $B_1 - A_1 \cong 13.7$, which indicates that the negative trend between Al/Si and $w_{s,\mathrm{floc}}$ occurs because the breakage rate exponent exceeds the aggregation rate exponent ($B_1 > A_1$). We expect that A_1 is positive because Al/Si is correlated with higher clay mineral abundance, and clays with stronger surface charges promote flocculation (Mehta & McAnally, 2008; van Olphen and Hsu, 1977). If $A_1 > 0$, then our analysis implies that $B_1 > 13.7$. In other words, the floc breakage rate is increasingly sensitive to Al/Si at greater values of Al/Si. We speculated two explanations. First, Equation (16) shows that $w_{s,floc} \propto D_t^2$, suggesting that the inclusion of progressively coarser sediment into flocs has a strong control on increasing floc settling velocity and vice versa. Clay might flocculate more readily than coarser sediment because it is more cohesive, so greater clay abundance (correlated with greater Al/Si) might cause clay-rich flocs and exclude coarser grain sizes (smaller D_t) thus reducing floc settling velocity. For a given floc size, flocs composed of smaller, high Al/Si primary particles must necessarily have more interparticle contacts and thus may be more fragile and prone to breakage in a turbulent fluid. We found evidence for this idea in the fact that (normalized) floc cutoff diameter varies inversely with Al/Si, indicating coarser grain sizes were increasingly excluded from flocs at higher Al/Si (Figure 9a).

A second possible reason for the greater sensitivity of floc breakage to larger Al/Si could be tied to the prevalence of a flat orientation of adsorbed organic matter on sediment. This orientation might be common in sedi-

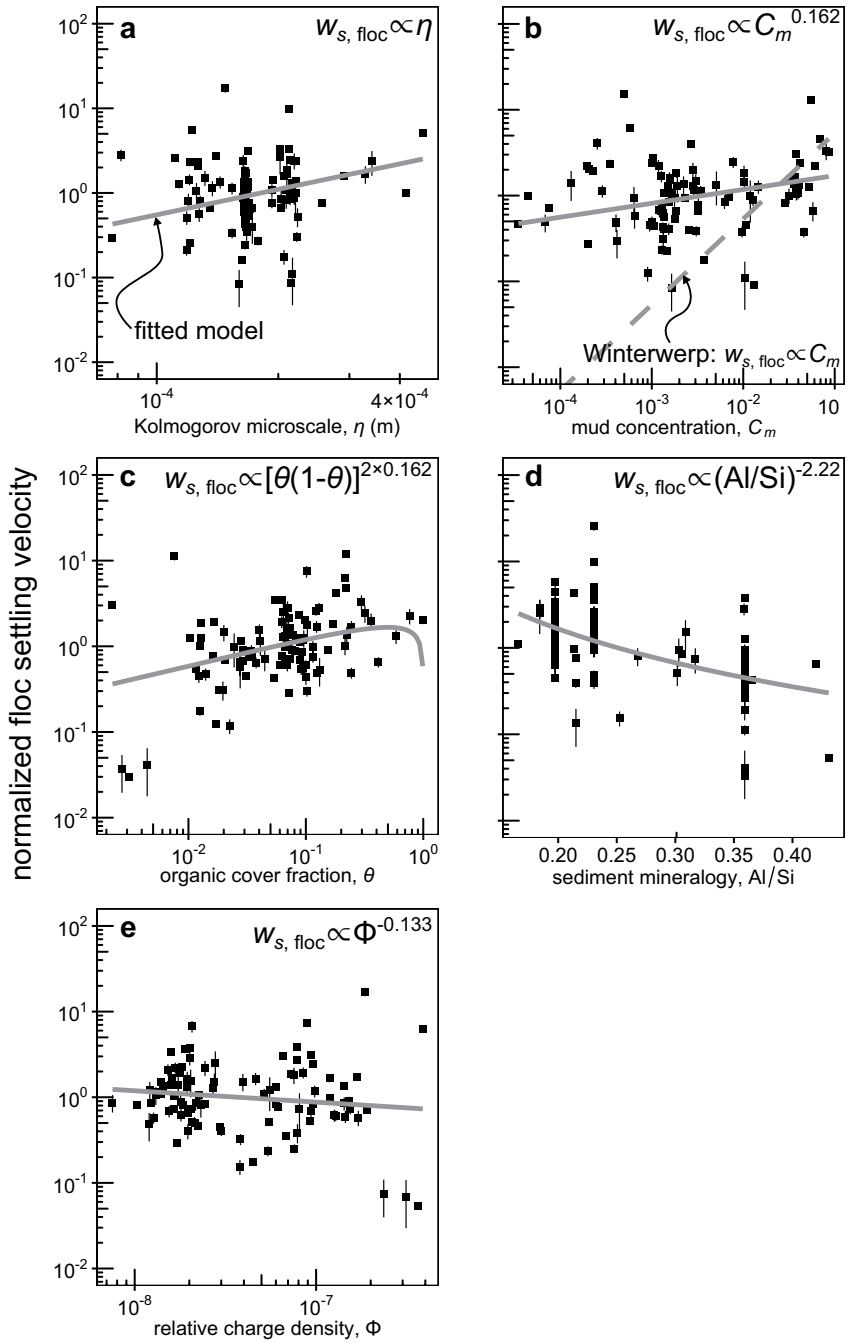

Figure 8. Individual parameters plotted against floc settling velocity, $w_{s,\mathrm{floc}}$, data normalized by the effects of all other predictors in the fitted $w_{s,\mathrm{floc}}$ model (Equation 23). In all panels, the solid line, labeled in panel a, indicates the fitted relationship (Table 2). In panel b, the dashed line is the prediction from the equilibrium Winterwerp model. Error bars represent the propagated 68% confidence interval.

ment with high specific surface area, like high Al/Si clay, because they have more adsorption sites to increase the chance of organic matter adsorbing to multiple sites on the same grain. However, a flat orientation is less effective for flocculation due to the lower probability of organic matter interacting with nearby particles (Gregory, 1978; Healy & La Mer, 1962). Thus, clay might have diminished sensitivity of floc aggregation to Al/Si (smaller A_1) and weaker floc structure (larger B_1). A flat orientation might also be less effective at capturing and retaining larger grains in flocs. Polymer chemistry and structure could also play a role by setting the binding strength to

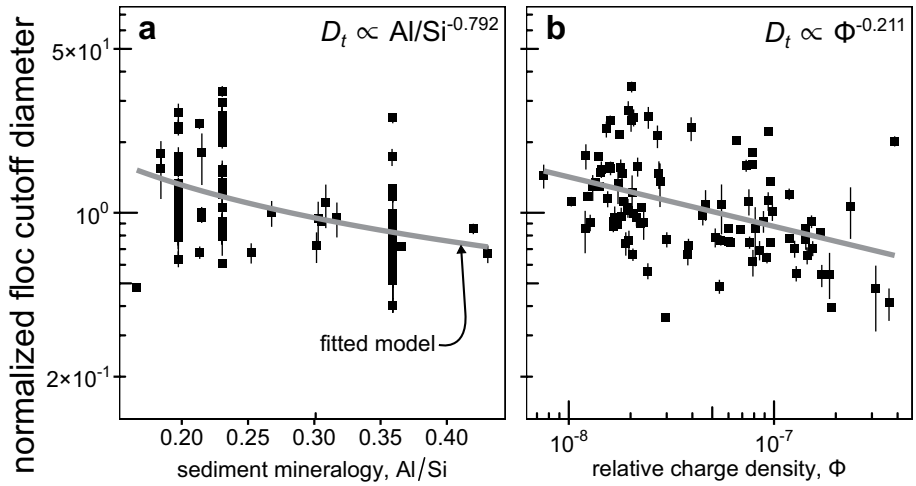

Figure 9. Sediment Al/Si (panel a) and relative charge density Φ (panel b) plotted against floc cutoff diameter, D_t, normalized by the effects of all other predictors in the fitted D_t model (Equation 18). The normalized values were further scaled by dividing the median to better compare each variable. In all panels, the solid line, labeled in panel a, indicates the fitted relationship (Table 2).

surface sites through mineralogy-specific interactions (Furukawa et al., 2014; Hemingway et al., 2019; Zeichner et al., 2021).

The relative charge density, Φ, displays a negative correlation with $w_{s,\mathrm{floc}}$ (exponent $s = -0.133 \pm 0.253$; Figure 8e). This relationship opposes the conventional idea that greater salinity enhances flocculation (e.g., Mehta & McAnally, 2008; van Leussen, 1988). The exponent on Φ is defined as $s = (B_2 - A_2)/(2j)$ (Equation 10) where A_2 and B_2 are the respective power-law aggregation and breakage exponents (Equations 7 and 8). Similar to the rationale for interpreting Al/Si, we estimated $j = -3.09$ so we must have $B_2 > A_2$. We again expected $A_2 > 0$ because greater ionic strength and Φ typically increase the ability of van der Waals attraction to aggregate sediment grains in the perspective of salinity-driven flocculation (Mehta & McAnally, 2008; Seiphoori et al., 2021). Assuming $A_2 > 0$, we have $B_2 > 0.82$. Although flocs are more sensitive to breakage with increasing salinity only if $B_2 > 1$, we expected that B_2 indeed exceeds 1 because $B_2 > 1$ is consistent with the D_t and D_f models where the estimated s is statistically significant. We propose that salinity could have similar interactions as Al/Si on floc size and settling velocity. First, greater ionic strength should primarily affect the flocculation of clay, on which negative surface charges are concentrated compared to coarser grain sizes. However, the bulk of mud in rivers is silt, for which ionic effects should be weaker (Table 2). Thus, larger Φ might preferentially flocculate clay, rather than silt, leading to more fragile flocs with a greater number of contact points. The inverse relationship between D_t and Φ is consistent with clay enrichment by excluding coarser silt from flocs at larger Φ (Figure 9b). Second, higher Φ could affect the physical organic matter orientation and organic matter binding capacity on sediment (e.g., through competition of ions and organic matter for binding sites on sediment surfaces).

In summary, the model calibration reveals that, out of the fitted parameters, D_t, $w_{s,\mathrm{floc}}$, and D_f in rivers are most sensitive to sediment Al/Si and relative charge density, Φ, because their exponent magnitudes are largest (Table 2). This fact should not be interpreted to mean that C_m and θ are less important mechanistically for flocculation because these variables might be correlated, a possibility that is masked in our calibration. The model also depends on η to a relatively large positive power (0.5 for D_t; 1 for $w_{s,\mathrm{floc}}$, and D_f) based on theory.

5. Discussion

Our results show that mud flocculation is widespread in rivers from geographically diverse regions spanning heterogeneous catchment lithologies and climates. Here we considered how flocculation might interplay with mud transport kinematics, channel morphology, organic carbon, tectonics, and climate.

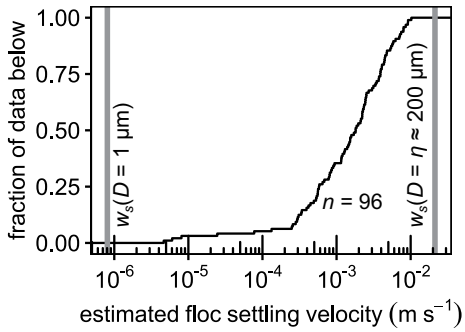

Figure 10. Empirical cumulative distribution function of river floc settling velocity estimates from the suspended sediment concentration-depth profile data compilation. The vertical lines indicate possible bounds on floc settling velocity in rivers: at 1-μm clay and at Kolmogorov microscale, η, of 200 μm typical of rivers and assuming solid particles ($n_f = 3$). We computed the settling velocity bounds using the model of Ferguson and Church (2004) (Section 3.1).

5.1. Mud Transport Kinematics

Flocculation in rivers greatly increases mud settling velocity up to orders-of-magnitude larger than rates for individual particles (Figure 4a). The total range of observed floc settling velocities is likely set by the primary particle diameter and Kolmogorov microscale. The minimum floc settling velocity simply occurs in the limit of increasingly fewer primary particles until the floc converges to a single particle settling according to Stokes theory. For an upper bound, prior work suggests that the Kolmogorov microscale sets the maximum floc diameter (e.g., Coufort et al., 2005; Kumar et al., 2010; Kuprenas et al., 2018). Our data compilation indicates a typical Kolmogorov microscale of 200 μm with a relatively narrow distribution across different rivers (Figures 5 and 6; Table 1), from which we calculated a maximal floc settling velocity assuming a solid particle ($n_f = 3$; Figure 10). Our data support the plausibility of these bounds because they bracket all of our floc settling velocity observations (Figure 10).

Enhanced mud settling velocity due to flocculation reduces mud advective transport lengths, with implications for setting the spatial distribution and rates of mud accretion and retention in depositional zones (e.g., floodplains, deltas, wetlands). The enhanced settling velocity of mud flocs might also cause mud to be exchanged between the flow and bed as suspended bed-material load rather than washload in alluvial rivers (Lamb et al., 2020). As a result, a dynamic equilibrium of suspended mud in rivers could lead to predictive mud flux models based on bed grain size distribution as are common for cohesionless sediment (Lamb et al., 2020; Ma et al., 2020).

5.2. River Channel-Scale Geomorphology

We found Kolmogorov microscale to be an important predictor of floc parameters relative to other factors, scaling linearly with floc settling velocity and diameter (Table 2). Channel hydraulic geometry (e.g., water depth and channel slope) controls the observed variation in shear velocity and Kolmogorov microscale between sites. Extremes in shear velocity inhibit mud flocculation because more intense turbulence reduces Kolmogorov microscale and less turbulent flows are less effective at suspending sediment and driving particle collisions. All else being equal, floc diameter and settling velocity might peak at moderate flows and shear velocities leading to higher relative contribution to mud accretion at those conditions. For example, repeat concentration-depth profiles sampled from 2012 to 2014 in the Fraser river show, at an intermediate flow, maximum floc settling velocity about 2.5 times greater than that at the lowest and highest flows (Environment Canada, 2021; Haught et al., 2017, Figure 11). Discharge also covaries with other biogeochemical factors in rivers, complicating the relationship between discharge and floc properties. For instance, floods tend to dilute dissolved load concentrations (e.g., Torres et al., 2015), which could promote larger flocs and offset floc breakage.

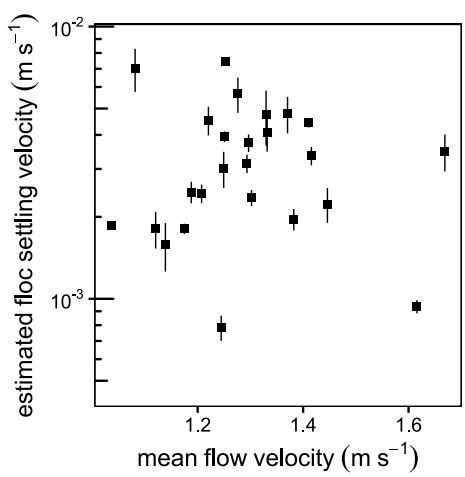

Figure 11. Comparison of mean flow velocity and floc settling velocity, estimated from our data compilation, for the Fraser River (Haught et al., 2017). We calculated mean flow velocity from continuity using channel width and depth (Haught et al., 2017) and water discharge at the Mission gaging station (station number 08MH024; Environment Canada, 2021).

Faster mud settling due to flocculation could contribute to finer channel-proximal deposits during overbank flow (Zeichner et al., 2021), and might help explain the existence of muddy levees (e.g., Adams et al., 2004; Nicholas & Walling, 1996). More cohesive channel-proximal deposits strengthen banks and limit channel lateral migration rates (Ielpi & Lapôtre, 2019; Peakall et al., 2007; van Dijk et al., 2013), thereby establishing a morphodynamic feedback between mud deposition and the long-term evolution of channel and floodplain morphology (Dunne & Jerolmack, 2020; Lapôtre et al., 2019). Mud flocculation could thus be an important control on equilibrium channel width in lowland alluvial rivers and river planform geometry. Over geologic time, mud flocculation could influence the development of alluvial stratigraphic architecture (Mackey & Bridge, 1995; Nicholas & Walling, 1996). More cohesive banks might favor aggradation and avulsion rather than lateral migration, leading to a mudrock-dominated alluvial architecture with sparse

sandy channel bodies rather than laterally extensive amalgamated channel belts (Jerolmack & Mohrig, 2007; Zeichner et al., 2021).

More accurate modeling of flocculation across floodplains with relatively slow flow likely requires the time-dependent flocculation model (Equation 9), rather than the equilibrium model on which we focused here for channels. The importance of using the unsteady model relies on the relative timescales of variation in Kolmogorov microscale and floc equilibration to local conditions, which we expect are comparable to each other in floodplains. Key parameters (n_f, j, k'_A, k'_B, A_1, A_2, B_1, B_2) remain to be evaluated in the time-dependent model in rivers.

5.3. Organic Carbon

Organic carbon flux in rivers is closely tied to mud because its high specific surface area provides ample sites to host particulate organic carbon (France-Lanord & Derry, 1997; Galy et al., 2008; Schlünz & Schneider, 2000). We found that binding of organic matter to mud is an important predictor for floc diameter and settling velocity through θ. The functional form of θ in the model indicates an optimum for the largest and fastest-settling flocs at $\theta = 0.5$. The bulk of our θ estimates lies in the regime of $\theta < 0.5$ in which increasing organic cover leads to larger floc size and settling velocity (Figure 6d). In this regime, the model predicts that river suspended sediment with greater organic carbon concentration form larger, faster-settling flocs. Thus, there is potential for a feedback in net depositional zones whereby higher organic carbon concentration causes faster floc and organic carbon settling rates, which increase carbon preservation potential (Galy et al., 2007; Hartnett et al., 1998; Torres et al., 2020).

Field and laboratory flocculation studies have indicated that organic matter composition can be important for determining the degree to which organic matter affects flocculation (e.g., Furukawa et al., 2014; Lee et al., 2017; Zeichner et al., 2021), an effect not accounted for in our model. Previous work suggested that bacteria-derived EPS tends to encourage flocculation because its molecular composition and structure can generate a chain-like physical orientation when adsorbed on sediment, while aromatic-rich materials tend to discourage flocculation because they coat sediment evenly and limit interparticle contact between organic matter and bare sediment surfaces (Furukawa et al., 2014; Healy & La Mer, 1962; Lee et al., 2019). Shifts in organic matter composition and/or abundance (i.e., due to changes in terrestrial vegetation, algal productivity, hillslope input of organic detritus) and the covariation of such factors due to climate change and human activity (e.g., Li et al., 2021) could trigger changes in flocculation. Floods are an additional catchment-specific factor for organic matter because floods of different magnitude can source different parts of the catchment (e.g., Dunne & Black, 1970) with different types of organic matter (Golombek et al., 2021).

Our results indicate that greater river water ionic strength, through Φ, reduces floc size in rivers. However, as rivers approach the ocean in estuaries, it is well known that the increasing salinity typically enhances flocculation. The salinity to induce flocculation usually occurs at a few parts per thousand (e.g., Drake, 1976; Einstein & Krone, 1962; Whitehouse et al., 2013), which is an order of magnitude larger than the values measured in rivers in our compilation (median salinity of 0.2 parts per thousand). Given that flocculation appears common in rivers, there could be a process transition from organics-mediated flocculation in freshwater to salinity-mediated flocculation in estuaries. In line with this view, Eisma et al. (1991) analyzed C isotope ratios of suspended sediment organic matter and found a transition in organic matter from freshwater-to marine-origin entering the Gironde estuary. In contrast, data from the Rhine and Elbe estuaries show that organic matter binding river flocs persisted in estuaries and led to minimal change in floc size in estuaries (Eisma et al., 1982; Puls & Kühl, 1986).

5.4. Climate, Tectonics, and Lithology

Climate, tectonics, and lithology affect chemical weathering and the delivery of weathering products (solids and solutes) to rivers, setting the chemical composition of sediment and river water (Hilton & West, 2020; West et al., 2005). In our model, these basinwide geochemical effects are expressed in Al/Si, Φ, and θ. Weathering-limited catchments (e.g., in rapidly uplifting mountains) yield fresher, less weathered sediment with smaller Al/Si and supply fewer dissolved ions (smaller Φ) to a river system (West et al., 2005). The rock and soil composition of source areas can also affect the composition and concentration of dissolved species in river water, which both contribute to Φ. Organic matter concentration in rivers might be higher in areas with more humid climates and/or relatively younger organics-rich soils and promote flocculation because of greater biological productivity and θ (Galy et al., 2015). Tectonic uplift, in concert with climate, could enhance mountain export of sediment

load, weathering products, and nutrients, which could also promote biological productivity (Geider et al., 2001; Godard et al., 2014; Raymo & Ruddiman, 1992).

With climate warming, rivers might source more weathering products and dissolved ions (Li et al., 2016; Perron, 2017), reducing the settling velocity of mud flocs in rivers. Warming could also change the magnitudes of sediment and organic carbon supply to rivers because of changes in catchment erosion rates (e.g., Perron, 2017) and biological productivity (e.g., Godard et al., 2014). These scenarios could alter the rates of mud and organic carbon delivery to floodplains via flocs and could be explored using our calibrated model.

6. Conclusion

Evidence from a global river suspended sediment data compilation shows that mud flocculation in rivers is common. Results from fitting the Rouse-Vanoni equation to grain size-specific concentration-depth profiles show, on average, that mud flocs in rivers have diameter of 130 μm, settle at a rate of 1.8 mm s^{-1}, and are composed of primary particles smaller than 39 μm (clay and silt). We proposed and verified a semi-empirical model for floc diameter and settling velocity in rivers. The calibrated model explains the estimated river floc settling velocities within a factor of about two. Out of the variables considered, sediment Al/Si has the strongest negative correlation with a fitted model exponent -2.22 ± 0.916. Kolmogorov microscale has the strongest positive correlation because it scales linearly with floc settling velocity. Higher floc settling velocity also scales with smaller relative charge density of river water compared to sediment (exponent -0.133 ± 0.253) and larger mud concentration and organic matter coverage on sediment grains (shared exponent 0.162 ± 0.0905). These relationships highlight the key role of geochemical interactions between primary particles and organic matter. Our model predicts a turbulence control for which floc diameter is generally smaller than the Kolmogorov microscale because floc breakage rate rapidly increases at large floc diameter, but floc diameter can exceed the microscale depending on the effects of the other predictor variables. The model dependencies imply that allogenic controls can affect floc properties, mud and organic carbon accretion in floodplains, and fluvial morphodynamics, resulting in possible new links between mud transport, tectonics, climate, and the global carbon cycle.

Notation

Al/Si	aluminum-silicon molar ratio of suspended sediment, dimensionless
C	Volumetric sediment concentration, dimensionless
C_{bi}	Volumetric near-bed sediment concentration for *i*th grain size class, dimensionless
C_m	Volumetric depth-averaged mud concentration, dimensionless
D	Particle diameter (unflocculated sediment), m
D_f	Floc diameter, m
D_p	Primary particle diameter, m
D_t	Floc cutoff diameter, m
e	Elementary charge magnitude ($= 1.602 \times 10^{-19}$), C
g	Gravitational acceleration ($= 9.81$ m s^{-2}), m s^{-2}
h	River water depth, m
h_b	Near-bed reference height, m
k	Calibrated model prefactor constant, dimensionless
k_A	Floc aggregation efficiency, dimensionless
k_B	Floc breakage efficiency, dimensionless
k_{BM}	Boltzmann constant ($= 1.381$), J K^{-1}
n_f	Floc fractal dimension ($= 2$), dimensionless
p_i	Rouse number for *i*th grain size class, dimensionless
q	Calibrated model exponent of $C_m\theta^2(1-\theta)^2$ term, dimensionless
r	Calibrated model exponent of Al/Si term, dimensionless
s	Calibrated model exponent of Φ term, dimensionless
u_*	Shear velocity, m s^{-1}
$w_{s,\mathrm{floc}}$	Floc settling velocity, m s^{-1}
w_{si}	*In situ* particle settling velocity for *i*th grain size class, m s^{-1}

β_i	Ratio of sediment and fluid diffusivities for ith grain size class, dimensionless
ϵ_0	Vacuum permittivity (= 8.854×10^{-12}), F m^{-1}
ϵ_r	Dielectric constant of water, dimensionless
η	Kolmogorov microscale, m
θ	Fraction of sediment surface covered by organic matter, dimensionless
Φ	Ratio of charge densities in river water and on the sediment
κ	Von Kármán constant (= 0.41), dimensionless
λ	Debye length, m
ν	Kinematic viscosity of water (= 10^{-6}), m^2 s^{-1}
ρ	Water density (= 1000), kg m^{-3}
ρ_s	Sediment density (= 2650), kg m^{-3}

Data Availability Statement

The suspended sediment concentration-depth profile, grain size distribution, and geochemical data used in this paper are freely available in the respective original publications. The authors are grateful to J. Bouchez, E. Dingle, and J. Shelley for sharing data used in this paper. Derived data are available online at https://doi.org/10.22002/D1.8962.

Acknowledgments
JN acknowledges NASA FINESST Grant 80NSSC20K1645. WWF and MPL acknowledge funding by the Discovery Fund and the Resnick Sustainability Institute at Caltech. GKL acknowledges the Caltech Geology Option Postdoc Fellowship. MPL acknowledges funding from the NASA Delta-X project by the Science Mission Directorate's Earth Science Division through the Earth Venture Suborbital-3 Program NNH17ZDA001N-EVS3 and the National Science Foundation Geomorphology and Land-use Dynamics Grant No. 2136991. The authors thank reviewer Scott Wright and four anonymous reviewers for their feedback, which improved the paper. The authors also thank Editor Ton Hoitink and Associate Editor Florent Grasso.

References

Abraham, D., Ramos-Villanueva, M., Pratt, T., Ganesh, N., May, D., Butler, W., et al. (2017). *Sediment and hydraulic measurements with computed bed load on the Missouri river, sioux city to hermann, 2014*. U. S. Army corps of engineers ERDC coastal and hydraulics laboratory.

Adams, P. N., Slingerland, R. L., & Smith, N. D. (2004). Variations in natural levee morphology in anastomosed channel flood plain complexes. *Geomorphology*, *61*(1), 127–142. https://doi.org/10.1016/j.geomorph.2003.10.005

Aller, R. C. (1998). Mobile deltaic and continental shelf muds as suboxic, fluidized bed reactors. *Marine Chemistry*, *61*(3–4), 143–155. https://doi.org/10.1016/S0304-4203(98)00024-3

Bache, D. H. (2004). Floc rupture and turbulence: A framework for analysis. *Chemical Engineering Science*, *59*(12), 2521–2534. https://doi.org/10.1016/j.ces.2004.01.055

Barber, A., Brandes, J., Leri, A., Lalonde, K., Balind, K., Wirick, S., et al. (2017). Preservation of organic matter in marine sediments by inner-sphere interactions with reactive iron. *Scientific Reports*, *7*(1), 1–10. https://doi.org/10.1038/s41598-017-00494-0

Baronas, J. J., Stevenson, E. I., Hackney, C. R., Darby, S. E., Bickle, M. J., Hilton, R. G., et al. (2020). Integrating suspended sediment flux in large alluvial river channels: Application of a synoptic Rouse-based model to the Irrawaddy and Salween rivers. *Journal of Geophysical Research: Earth Surface*, *125*(9), e2020JF005554. https://doi.org/10.1029/2020JF005554

Bock, M. J., & Mayer, L. M. (2000). Mesodensity organo–clay associations in a near-shore sediment. *Marine Geology*, *163*(1–4), 65–75. https://doi.org/10.1016/S0025-3227(99)00105-X

Bouchez, J. (2022). *Grain size distribution of Amazon River sediment samples collected over the period 2005–2008; and ADCP water velocity profiles collected on the major tributaries of the Amazon in Bolivia and Peru, 2007-2008*. https://doi.org/10.5281/zenodo.6458298

Bouchez, J., Gaillardet, J., Lupker, M., Louvat, P., France-Lanord, C., Maurice, L., et al. (2012). Floodplains of large rivers: Weathering reactors or simple silos? *Chemical Geology*, *332*, 166–184. https://doi.org/10.1016/j.chemgeo.2012.09.032

Bouchez, J., Lupker, M., Gaillardet, J., France-Lanord, C., & Maurice, L. (2011). How important is it to integrate riverine suspended sediment chemical composition with depth? Clues from Amazon River depth-profiles. *Geochimica et Cosmochimica Acta*, *75*(22), 6955–6970. https://doi.org/10.1016/j.gca.2011.08.038

Bouchez, J., Métivier, F., Lupker, M., Maurice, L., Perez, M., Gaillardet, J., & France-Lanord, C. (2011). Prediction of depth-integrated fluxes of suspended sediment in the Amazon River: Particle aggregation as a complicating factor. *Hydrological Processes*, *25*(5), 778–794. https://doi.org/10.1002/hyp.7868

Brigham, C. (2018). Biopolymers: Biodegradable alternatives to traditional plastics. *Green Chemistry: An Inclusive Approach*, 753–770. https://doi.org/10.1016/B978-0-12-809270-5.00027-3

Bungartz, H., Krüger, A., & Engelhardt, C. (2006). Fluvial suspended sediment dynamics: Implications for particulate organic carbon transport modeling. *Water Resources Research*, *42*(10). https://doi.org/10.1029/2005WR004486

Bungartz, H., & Wanner, S. C. (2004). Significance of particle interaction to the modelling of cohesive sediment transport in rivers. *Hydrological Processes*, *18*(9), 1685–1702. https://doi.org/10.1002/hyp.1412

Burban, P.-Y., Xu, Y.-J., McNeil, J., & Lick, W. (1990). Settling speeds of flocs in fresh water and seawater. *Journal of Geophysical Research*, *95*(C10), 18213–18220. https://doi.org/10.1029/JC095iC10p18213

Chase, R. R. (1979). Settling behavior of natural aquatic particulates. *Limnology & Oceanography*, *24*(3), 417–426. https://doi.org/10.4319/lo.1979.24.3.0417

Church, M. (2006). Bed material transport and the morphology of alluvial river channels. *Annual Review of Earth and Planetary Sciences*, *34*(1), 325–354. https://doi.org/10.1146/annurev.earth.33.092203.122721

Coufort, C., Bouyer, D., & Liné, A. (2005). Flocculation related to local hydrodynamics in a Taylor–Couette reactor and in a jar. *Chemical Engineering Science*, *60*(8–9), 2179–2192. https://doi.org/10.1016/j.ces.2004.10.038

Dingle, E. H. (2021). *Karnali River Suspended Sediment Sampling*. https://doi.org/10.5281/zenodo.4923989

Dingle, E. H., Sinclair, H. D., Venditti, J. G., Attal, M., Kinnaird, T. C., Creed, M., et al. (2020). Sediment dynamics across gravel-sand transitions: Implications for river stability and floodplain recycling. *Geology*, *48*(5), 468–472. https://doi.org/10.1130/G46909.1

Drake, D. E. (1976). Suspended sediment transport and mud deposition on continental shelves. *Marine Sediment Transport and Environmental Management*, *40*, 127–158.

Droppo, I. G., Leppard, G. G., Flannigan, D. T., & Liss, S. N. (1997). The freshwater floc: A functional relationship of water and organic and inorganic floc constituents affecting suspended sediment properties. *The Interactions between Sediments and Water: Proceedings of the 7th International Symposium, Baveno, Italy 22–25 September*, *1996*, 43–53. https://doi.org/10.1007/978-94-011-5552-6._5

Droppo, I. G., & Ongley, E. D. (1994). Flocculation of suspended sediment in rivers of southeastern Canada. *Water Research*, *28*(8), 1799–1809. https://doi.org/10.1016/0043-1354(94)90253-4

Dunne, K. B., & Jerolmack, D. J. (2020). What sets river width? *Science Advances*, *6*(41), eabc1505. https://doi.org/10.1126/sciadv.abc1505

Dunne, T., & Black, R. D. (1970). Partial area contributions to storm runoff in a small New England watershed. *Water Resources Research*, *6*(5), 1296–1311. https://doi.org/10.1029/WR006i005p01296

Einstein, H. A., & Krone, R. B. (1962). Experiments to determine modes of cohesive sediment transport in salt water. *Journal of Geophysical Research*, *67*(4), 1451–1461. https://doi.org/10.1029/JZ067i004p01451

Eisma, D., Bernard, P., Cadée, G. C., Ittekkot, V., Kalf, J., Laane, R., et al. (1991). Suspended-matter particle size in some West-European estuaries; Part I: Particle-size distribution. *Netherlands Journal of Sea Research*, *28*(3), 193–214. https://doi.org/10.1016/0077-7579(91)90017-U

Eisma, D., Cadée, G. C., Laane, R., & Kalf, J. (1982). Preliminary results of AURELIA-and NAVICULA cruises in the Rhine-and Ems-estuaries, January-February, 1982. *Mitteilungen aus dem Geologisch-Palaontologischen Institut der Universitat Hamburg*, *52*, 633–654.

Environment Canada. (2021). *Environment and climate change Canada historical hydrometric data*. Retrieved from https://wateroffice.ec.gc.ca/mainmenu/historical_data_index_e.html

Ersahin, S., Gunal, H., Kutlu, T., Yetgin, B., & Coban, S. (2006). Estimating specific surface area and cation exchange capacity in soils using fractal dimension of particle-size distribution. *Geoderma*, *136*(3–4), 588–597. https://doi.org/10.1016/j.geoderma.2006.04.014

Ferguson, R. I., & Church, M. (2004). A simple universal equation for grain settling velocity. *Journal of Sedimentary Research*, *74*(6), 933–937. https://doi.org/10.1306/051204740933

France-Lanord, C., & Derry, L. A. (1997). Organic carbon burial forcing of the carbon cycle from Himalayan erosion. *Nature*, *390*(6655), 65–67. https://doi.org/10.1038/36324

Furukawa, Y., Reed, A. H., & Zhang, G. (2014). Effect of organic matter on estuarine flocculation: A laboratory study using montmorillonite, humic acid, xanthan gum, guar gum and natural estuarine flocs. *Geochemical Transactions*, *15*(1). https://doi.org/10.1186/1467-4866-15-1

Galy, V., France-Lanord, C., Beyssac, O., Faure, P., Kudrass, H., & Palhol, F. (2007). Efficient organic carbon burial in the Bengal fan sustained by the Himalayan erosional system. *Nature*, *450*(7168), 407–410. https://doi.org/10.1038/nature06273

Galy, V., France-Lanord, C., & Lartiges, B. (2008). Loading and fate of particulate organic carbon from the Himalaya to the Ganga–Brahmaputra delta. *Geochimica et Cosmochimica Acta*, *72*(7), 1767–1787. https://doi.org/10.1016/j.gca.2008.01.027

Galy, V., Peucker-Ehrenbrink, B., & Eglinton, T. (2015). Global carbon export from the terrestrial biosphere controlled by erosion. *Nature*, *521*(7551), 204–207. https://doi.org/10.1038/nature14400

Garcia, M. (2008). *Sedimentation Engineering: Processes, Measurements, Modeling, and Practice*. https://doi.org/10.1061/9780784408148

Garcia-Aragon, J., Droppo, I. G., Krishnappan, B., Trapp, B., & Jaskot, C. (2011). Experimental assessment of Athabasca River cohesive sediment deposition dynamics. *Water Quality Research Journal of Canada*, *46*(1), 87–96. https://doi.org/10.2166/wqrjc.2011.030

Geider, R. J., Delucia, E. H., Falkowski, P. G., Finzi, A. C., Grime, J. P., Grace, J., et al. (2001). Primary productivity of planet Earth: Biological determinants and physical constraints in terrestrial and aquatic habitats. *Global Change Biology*, *7*(8), 849–882. https://doi.org/10.1046/j.1365-2486.2001.00448.x

Gerbersdorf, S. U., Jancke, T., Westrich, B., & Paterson, D. M. (2008). Microbial stabilization of riverine sediments by extracellular polymeric substances. *Geobiology*, *6*(1), 57–69. https://doi.org/10.1111/j.1472-4669.2007.00120.x

Godard, V., Bourlès, D. L., Spinabella, F., Burbank, D. W., Bookhagen, B., Fisher, G. B., et al. (2014). Dominance of tectonics over climate in Himalayan denudation. *Geology*, *42*(3), 243–246. https://doi.org/10.1130/G35342.1

Golombek, N. Y., Scheingross, J. S., Repasch, M. N., Hovius, N., Menges, J., Sachse, D., et al. (2021). Fluvial organic carbon composition regulated by seasonal variability in lowland river migration and water discharge. *Geophysical Research Letters*, *48*(24), e2021GL093416. https://doi.org/10.1029/2021GL093416

Graf, W. H., & Cellino, M. (2002). Suspension flows in open channels; experimental study. *Journal of Hydraulic Research*, *40*(4), 435–447. https://doi.org/10.1080/00221680209499886

Gratiot, N., Michallet, H., & Mory, M. (2005). On the determination of the settling flux of cohesive sediments in a turbulent fluid. *Journal of Geophysical Research*, *110*(C6), C06004. https://doi.org/10.1029/2004JC002732

Gregory, J. (1978). Effects of polymers on colloid stability. *The Scientific Basis of Flocculation*, 101–130. https://doi.org/10.1007/978-94-009-9938-1_6

Hackley, P. C., Valentine, B. J., Voortman, L. M., Van Oosten Slingeland, D. S., & Hatcherian, J. (2017). Utilization of integrated correlative light and electron microscopy (iCLEM) for imaging sedimentary organic matter. *Journal of Microscopy*, *267*(3), 371–383. https://doi.org/10.1111/jmi.12576

Hartnett, H. E., Keil, R. G., Hedges, J. I., & Devol, A. H. (1998). Influence of oxygen exposure time on organic carbon preservation in continental margin sediments. *Nature*, *391*(6667), 572–575. https://doi.org/10.1038/35351

Haught, D., Venditti, J. G., & Wright, S. A. (2017). Calculation of in situ acoustic sediment attenuation using off-the-shelf horizontal ADCPs in low concentration settings. *Water Resources Research*, *53*(6), 5017–5037. https://doi.org/10.1002/2016WR019695

Healy, T. W., & La Mer, V. K. (1962). The adsorption-flocculation reactions of a polymer with an aqueous colloidal dispersion. *The Journal of Physical Chemistry*, *66*(10), 1835–1838. https://doi.org/10.1021/j100816a014

Hemingway, J. D., Rothman, D. H., Grant, K. E., Rosengard, S. Z., Eglinton, T. I., Derry, L. A., & Galy, V. V. (2019). Mineral protection regulates long-term global preservation of natural organic carbon. *Nature*, *570*(7760), 228–231. https://doi.org/10.1038/s41586-019-1280-6

Hill, P. S., Milligan, T. G., & Geyer, W. R. (2000). Controls on effective settling velocity of suspended sediment in the Eel River flood plume. *Continental Shelf Research*, *20*(16), 2095–2111. https://doi.org/10.1016/S0278-4343(00)00064-9

Hilton, R. G., & West, A. J. (2020). Mountains, erosion and the carbon cycle. *Nature Reviews Earth & Environment*, *1*(6), 284–299. https://doi.org/10.1038/s43017-020-0058-6

Ielpi, A., & Lapôtre, M. G. (2019). Biotic forcing militates against river meandering in the modern Bonneville Basin of Utah. *Sedimentology*, *66*(5), 1896–1929. https://doi.org/10.1111/sed.12562

Ito, A., & Wagai, R. (2017). Global distribution of clay-size minerals on land surface for biogeochemical and climatological studies. *Scientific Data*, *4*(1). https://doi.org/10.1038/sdata.2017.103

Jackson, M. L., Tyler, S. A., Willis, A. L., Bourbeau, G. A., & Pennington, R. P. (1948). Weathering sequence of clay-size minerals in soils and sediments. I. Fundamental generalizations. *The Journal of Physical Chemistry*, *52*(7), 1237–1260. https://doi.org/10.1021/j150463a015

Jerolmack, D. J., & Mohrig, D. (2007). Conditions for branching in depositional rivers. *Geology*, *35*(5), 463–466. https://doi.org/10.1130/G23308A.1

Kleinhans, M. G., de Vries, B., Braat, L., & van Oorschot, M. (2018). Living landscapes: Muddy and vegetated floodplain effects on fluvial pattern in an incised river. *Earth Surface Processes and Landforms*, *43*(14), 2948–2963. https://doi.org/10.1002/esp.4437

Kranck, K., & Milligan, T. (1980). Macroflocs: Production of marine snow in the laboratory. *Marine Ecology - Progress Series*, *3*, 19–24. https://doi.org/10.3354/meps003019

Kranenburg, C. (1994). The fractal structure of cohesive sediment aggregates. *Estuarine, Coastal and Shelf Science*, *39*(6), 451–460. https://doi.org/10.1016/S0272-7714(06)80002-8

Kumar, R. G., Strom, K. B., & Keyvani, A. (2010). Floc properties and settling velocity of San Jacinto estuary mud under variable shear and salinity conditions. *Continental Shelf Research*, *30*(20), 2067–2081. https://doi.org/10.1016/j.csr.2010.10.006

Kuprenas, R., Tran, D., & Strom, K. (2018). A shear-limited flocculation model for dynamically predicting average floc size. *Journal of Geophysical Research: Oceans*, *123*(9), 6736–6752. https://doi.org/10.1029/2018JC014154

Lamb, M. P., De Leeuw, J., Fischer, W. W., Moodie, A. J., Venditti, J. G., Nittrouer, J. A., et al. (2020). Mud in rivers transported as flocculated and suspended bed material. *Nature Geoscience*, *13*(8), 566–570. https://doi.org/10.1038/s41561-020-0602-5

Lapôtre, M. G., Ielpi, A., Lamb, M. P., Williams, R. M., & Knoll, A. H. (2019). Model for the Formation of Single-Thread Rivers in Barren Landscapes and Implications for Pre-Silurian and Martian Fluvial Deposits. *Journal of Geophysical Research: Earth Surface*, *124*(12), 2757–2777. https://doi.org/10.1029/2019JF005156

Larsen, L. G., Harvey, J. W., & Crimaldi, J. P. (2009). Morphologic and transport properties of natural organic floc. *Water Resources Research*, *45*(1). https://doi.org/10.1029/2008WR006990

Lee, B. J., Hur, J., & Toorman, E. A. (2017). Seasonal variation in flocculation potential of river water: Roles of the organic matter pool. *Water*, *9*(5), 335. https://doi.org/10.3390/w9050335

Lee, B. J., Kim, J., Hur, J., Choi, I. H., Toorman, E. A., Fettweis, M., & Choi, J. W. (2019). Seasonal dynamics of organic matter composition and its effects on suspended sediment flocculation in river water. *Water Resources Research*, *55*(8), 6968–6985. https://doi.org/10.1029/2018WR024486

Lehner, B., Verdin, K., & Jarvis, A. (2008). New global hydrography derived from spaceborne elevation data. *Eos, Transactions American Geophysical Union*, *89*(10), 93–94. https://doi.org/10.1029/2008EO100001

Li, G., Hartmann, J., Derry, L. A., West, A. J., You, C.-F., Long, X., et al. (2016). Temperature dependence of basalt weathering. *Earth and Planetary Science Letters*, *443*, 59–69. https://doi.org/10.1016/j.epsl.2016.03.015

Li, G. K., Fischer, W. W., Lamb, M. P., West, A. J., Zhang, T., Galy, V., et al. (2021). Coal fly ash is a major carbon flux in the Chang Jiang (Yangtze River) basin. *Proceedings of the National Academy of Sciences*, *118*(21). https://doi.org/10.1073/pnas.1921544118

Lick, W., & Lick, J. (1988). Aggregation and disaggregation of fine-grained lake sediments. *Journal of Great Lakes Research*, *14*(4), 514–523. https://doi.org/10.1016/S0380-1330(88)71583-X

Lupker, M., France-Lanord, C., Galy, V., Lavé, J., Gaillardet, J., Gajurel, A. P., et al. (2012). Predominant floodplain over mountain weathering of Himalayan sediments (Ganga basin). *Geochimica et Cosmochimica Acta*, *84*, 410–432. https://doi.org/10.1016/j.gca.2012.02.001

Lupker, M., France-Lanord, C., Lavé, J., Bouchez, J., Galy, V., Métivier, F., et al. (2011). A Rouse-based method to integrate the chemical composition of river sediments: Application to the Ganga basin. *Journal of Geophysical Research*, *116*(F4), F04012. https://doi.org/10.1029/2010JF001947

Ma, H., Nittrouer, J. A., Wu, B., Lamb, M. P., Zhang, Y., Mohrig, D., et al. (2020). Universal relation with regime transition for sediment transport in fine-grained rivers. *Proceedings of the National Academy of Sciences*, *117*(1), 171–176. https://doi.org/10.1073/pnas.1911225116

Mackey, S. D., & Bridge, J. S. (1995). Three-dimensional model of alluvial stratigraphy; theory and applications. *Journal of Sedimentary Research*, *65*(1b), 7–31. https://doi.org/10.1306/D42681D5-2B26-11D7-8648000102C1865D

Maggi, F. (2008). Stochastic flocculation of cohesive sediment: Analysis of floc mobility within the floc size spectrum. *Water Resources Research*, *44*(1). https://doi.org/10.1029/2007WR006109

Maggi, F. (2009). Biological flocculation of suspended particles in nutrient-rich aqueous ecosystems. *Journal of Hydrology*, *376*(1–2), 116–125. https://doi.org/10.1016/j.jhydrol.2009.07.040

Maggi, F., Mietta, F., & Winterwerp, J. C. (2007). Effect of variable fractal dimension on the floc size distribution of suspended cohesive sediment. *Journal of Hydrology*, *343*(1–2), 43–55. https://doi.org/10.1016/j.jhydrol.2007.05.035

Matsuo, T., & Unno, H. (1981). Forces acting on floc and strength of floc. *Journal of the Environmental Engineering Division*, *107*(3), 527–545. https://doi.org/10.1061/JEEGAV.0001174

Mayer, L. M. (1999). Extent of coverage of mineral surfaces by organic matter in marine sediments. *Geochimica et Cosmochimica Acta*, *63*(2), 207–215. https://doi.org/10.1016/S0016-7037(99)00028-9

McMahon, W. J., & Davies, N. S. (2018). Evolution of alluvial mudrock forced by early land plants. *Science*, *359*(6379), 1022–1024. https://doi.org/10.1126/science.aan4660

Meade, R. H. (1972). Transport and deposition of sediments in estuaries. *Geological Society of America*, *133*(1), 91–120. https://doi.org/10.1130/mem133-p91

Mehta, A. J., & McAnally, W. H. (2008). Fine grained sediment transport. *Sedimentation Engineering: Processes, Measurements, Modeling, and Practice*, 253–306. https://doi.org/10.1061/9780784408148

Mehta, A. J., & Partheniades, E. (1975). An investigation of the depositional properties of flocculated fine sediments. *Journal of Hydraulic Research*, *13*(4), 361–381. https://doi.org/10.1080/00221687509499694

Millar, R. G., & Quick, M. C. (1998). Stable width and depth of gravel-bed rivers with cohesive banks. *Journal of Hydraulic Engineering*, *124*(10), 1005–1013. https://doi.org/10.1061/(ASCE)0733-9429(1998)124

Molski, A. (1989). On the collision efficiency approach to flocculation. *Colloid & Polymer Science*, *267*(4), 371–375. https://doi.org/10.1007/BF01413632

Moodie, A. J., Nittrouer, J. A., Ma, H., Carlson, B. N., Wang, Y., Lamb, M. P., & Parker, G. (2020). Suspended-sediment induced stratification inferred from concentration and velocity profile measurements in the lower Yellow River, China. *Water Resources Research*, e2020WR027192. https://doi.org/10.1029/2020WR027192

Nezu, I., & Nakagawa, H. (1993). Turbulence in open-channel flows. *AA Balkema, Rotterdam*, 1–281.

Nicholas, A. P., & Walling, D. E. (1996). The significance of particle aggregation in the overbank deposition of suspended sediment on river floodplains. *Journal of Hydrology*, *186*(1–4), 275–293. https://doi.org/10.1016/S0022-1694(96)03023-5

Osborn, R., Dillon, B., Tran, D., Abolfazli, E., Dunne, K. B., Nittrouer, J. A., & Strom, K. (2021). FlocARAZI: An in-situ, image-based profiling instrument for sizing solid and flocculated suspended sediment. *Journal of Geophysical Research: Earth Surface*, *126*(11), e2021JF006210. https://doi.org/10.1029/2021JF006210

Osborn, R., Dunne, K. B. J., Abolfazli, E., Strom, K., & Nittrouer, J. A. (2020). Characterization of in-situ floc sizes over the vertical within the Mississippi river and its distributaries. *AGU Fall Meeting Abstracts*, *2020*, EP001–0005.

Owen, B. B., Miller, R. C., Milner, C. E., & Cogan, H. L. (1961). The dielectric constant of water as a function of temperature and pressure. *The Journal of Physical Chemistry*, *65*(11), 2065–2070. https://doi.org/10.1021/j100828a035
Paola, C., Parker, G., Seal, R., Sinha, S. K., Southard, J. B., & Wilcock, P. R. (1992). Downstream fining by selective deposition in a laboratory flume. *Science*, *258*(5089), 1757–1760. https://doi.org/10.1126/science.258.5089.1757
Peakall, J., Ashworth, P. J., & Best, J. L. (2007). Meander-bend evolution, alluvial architecture, and the role of cohesion in sinuous river channels: A flume study. *Journal of Sedimentary Research*, *77*(3), 197–212. https://doi.org/10.2110/jsr.2007.017
Perron, J. T. (2017). Climate and the pace of erosional landscape evolution. *Annual Review of Earth and Planetary Sciences*, *45*(1), 561–591. https://doi.org/10.1146/annurev-earth-060614-105405
Pizzuto, J., Schenk, E. R., Hupp, C. R., Gellis, A., Noe, G., Williamson, E., et al. (2014). Characteristic length scales and time-averaged transport velocities of suspended sediment in the mid-Atlantic Region, USA. *Water Resources Research*, *50*(2), 790–805. https://doi.org/10.1002/2013WR014485
Puls, W., & Kühl, H. (1986). Field measurements of the settling velocities of estuarine flocs. In *Proceedings of the 3rd international symposium on river sedimentation, the university of Mississippi* (pp. 525–536).
Ransom, B., Bennett, R. H., Baerwald, R., & Shea, K. (1997). TEM study of in situ organic matter on continental margins: Occurrence and the "monolayer" hypothesis. *Marine Geology*, *138*(1–2), 1–9. https://doi.org/10.1016/S0025-3227(97)00012-1
Raymo, M. E., & Ruddiman, W. F. (1992). Tectonic forcing of late Cenozoic climate. *Nature*, *359*(6391), 117–122. https://doi.org/10.1038/359117a0
Rommelfanger, N., Vowinckel, B., Wang, Z., Meiburg, E., & Luzzatto-Fegiz, P. (2020). A simple theory and experiments for onset of flocculation in kaolin clay suspensions. In *River flow 2020* (pp. 820–822). CRC Press.
Rouse, H. (1937). Modern conceptions of the mechanics of fluid turbulence. *Transactions of the American Society of Civil Engineers*, *102*(1), 463–505. https://doi.org/10.1061/TACEAT.0004872
Ruehrwein, R. A., & Ward, D. W. (1952). Mechanism of clay aggregation by polyelectrolytes. *Soil Science*, *73*(6), 485–492. https://doi.org/10.1097/00010694-195206000-00007
Santini, W., Camenen, B., Coz, J. L., Vauchel, P., Guyot, J.-L., Lavado, W., et al. (2019). An index concentration method for suspended load monitoring in large rivers of the Amazonian foreland. *Earth Surface Dynamics*, *7*(2), 515–536. https://doi.org/10.5194/esurf-7-515-2019
Schlünz, B., & Schneider, R. R. (2000). Transport of terrestrial organic carbon to the oceans by rivers: Re-estimating flux- and burial rates. *International Journal of Earth Sciences*, *88*(4), 599–606. https://doi.org/10.1007/s005310050290
Seiphoori, A., Gunn, A., Kosgodagan Acharige, S., Arratia, P. E., & Jerolmack, D. J. (2021). Tuning sedimentation through surface charge and particle shape. *Geophysical Research Letters*, *48*(7), e2020GL091251. https://doi.org/10.1029/2020GL091251
Smellie, R. H., & La Mer, V. K. (1958). Flocculation, subsidence and filtration of phosphate slimes: VI. A quantitative theory of filtration of flocculated suspensions. *Journal of Colloid Science*, *13*(6), 589–599. https://doi.org/10.1016/0095-8522(58)90071-0
Smith, J. D., & McLean, S. R. (1977). Spatially averaged flow over a wavy surface. *Journal of Geophysical Research*, *82*(12), 1735–1746. https://doi.org/10.1029/JC082i012p01735
Son, M., & Hsu, T.-J. (2008). Flocculation model of cohesive sediment using variable fractal dimension. *Environmental Fluid Mechanics*, *8*(1), 55–71. https://doi.org/10.1007/s10652-007-9050-7
Son, M., & Hsu, T.-J. (2011). The effects of flocculation and bed erodibility on modeling cohesive sediment resuspension. *Journal of Geophysical Research*, *116*(C3), C03021. https://doi.org/10.1029/2010JC006352
Spicer, P. T., & Pratsinis, S. E. (1996). Coagulation and fragmentation: Universal steady-state particle-size distribution. *AIChE Journal*, *42*(6), 1612–1620. https://doi.org/10.1002/aic.690420612
Strom, K., & Keyvani, A. (2011). An explicit full-range settling velocity equation for mud flocs. *Journal of Sedimentary Research*, *81*(12), 921–934. https://doi.org/10.2110/jsr.2011.62
Tambo, N., & Hozumi, H. (1979). Physical characteristics of flocs—II. Strength of floc. *Water Research*, *13*(5), 421–427. https://doi.org/10.1016/0043-1354(79)90034-4
Tambo, N., & Watanabe, Y. (1979). Physical aspect of flocculation process—I: Fundamental treatise. *Water Research*, *13*(5), 429–439. https://doi.org/10.1016/0043-1354(79)90035-6
Tang, F. H., & Maggi, F. (2016). A mesocosm experiment of suspended particulate matter dynamics in nutrient-and biomass-affected waters. *Water Research*, *89*, 76–86. https://doi.org/10.1016/j.watres.2015.11.033
Tennekes, H., & Lumley, J. L. (1972). *A first course in turbulence*. MIT Press.
Torres, M. A., Kemeny, P. C., Lamb, M. P., Cole, T. L., & Fischer, W. W. (2020). Long-term storage and age-biased export of fluvial organic carbon: Field evidence from west Iceland. *Geochemistry, Geophysics, Geosystems*, *21*(4), e2019GC008632. https://doi.org/10.1029/2019GC008632
Torres, M. A., West, A. J., & Clark, K. E. (2015). Geomorphic regime modulates hydrologic control of chemical weathering in the Andes–Amazon. *Geochimica et Cosmochimica Acta*, *166*, 105–128. https://doi.org/10.1016/j.gca.2015.06.007
Tsai, C.-H., Iacobellis, S., & Lick, W. (1987). Flocculation of fine-grained lake sediments due to a uniform shear stress. *Journal of Great Lakes Research*, *13*(2), 135–146. https://doi.org/10.1016/S0380-1330(87)71637-2
Van Dijk, W. M., Van de Lageweg, W. I., & Kleinhans, M. G. (2013). Formation of a cohesive floodplain in a dynamic experimental meandering river. *Earth Surface Processes and Landforms*, *38*(13), 1550–1565. https://doi.org/10.1002/esp.3400
Van Leussen, W. (1988). Aggregation of particles, settling velocity of mud flocs a review. *Physical Processes in Estuaries*, 347–403. https://doi.org/10.1007/978-3-642-73691-9_19
Van Olphen, H., & Hsu, P. H. (1977). *An introduction to clay colloid chemistry*. Wiley.
Verney, R., Lafite, R., & Brun-Cottan, J.-C. (2009). Flocculation potential of estuarine particles: The importance of environmental factors and of the spatial and seasonal variability of suspended particulate matter. *Estuaries and Coasts*, *32*(4), 678–693. https://doi.org/10.1007/s12237-009-9160-1
West, A. J., Galy, A., & Bickle, M. (2005). Tectonic and climatic controls on silicate weathering. *Earth and Planetary Science Letters*, *235*(1–2), 211–228. https://doi.org/10.1016/j.epsl.2005.03.020
Whitehouse, U. G., Jeffrey, L. M., & Debbrecht, J. D. (2013). Differential settling tendencies of clay minerals in saline waters. *Clays and Clay Minerals*, 1–79. https://doi.org/10.1016/B978-0-08-009235-5.50006-1
Wilcock, P. R. (1996). Estimating local bed shear stress from velocity observations. *Water Resources Research*, *32*(11), 3361–3366. https://doi.org/10.1029/96WR02277
Winterwerp, J. C. (1998). A simple model for turbulence induced flocculation of cohesive sediment. *Journal of Hydraulic Research*, *36*(3), 309–326. https://doi.org/10.1080/00221689809498621
Winterwerp, J. C. (2002). On the flocculation and settling velocity of estuarine mud. *Continental Shelf Research*, *22*(9), 1339–1360. https://doi.org/10.1016/S0278-4343(02)00010-9

Wright, S., & Parker, G. (2004). Flow resistance and suspended load in sand-bed rivers: Simplified stratification model. *Journal of Hydraulic Engineering*, *130*(8), 796–805. https://doi.org/10.1061/(ASCE)0733-9429(2004)130

Xu, F., Wang, D.-P., & Riemer, N. (2008). Modeling flocculation processes of fine-grained particles using a size-resolved method: Comparison with published laboratory experiments. *Continental Shelf Research*, *28*(19), 2668–2677. https://doi.org/10.1016/j.csr.2008.09.001

Zeichner, S. S., Nghiem, J., Lamb, M. P., Takashima, N., De Leeuw, J., Ganti, V., & Fischer, W. W. (2021). Early plant organics increased global terrestrial mud deposition through enhanced flocculation. *Science*, *371*(6528), 526–529. https://doi.org/10.1126/science.abd0379

References From the Supporting Information

Alexander, R. B., Ludtke, A. S., Fitzgerald, K. K., & Schertz, T. L. (1997). Data from selected U.S. Geological Survey national stream water-quality monitoring networks (WQN) on CD-ROM. In Data from selected U.S. *Geological Survey national stream water-quality monitoring networks (WQN) on CD-ROM*, 96–337. https://doi.org/10.3133/ofr96337. (USGS Numbered Series No; Open-File Report, Vols. 96–337).

Azam, M. M., Kumari, M., Maharana, C., Singh, A. K., & Tripathi, J. K. (2018). Recent insights into the dissolved and particulate fluxes from the Himalayan tributaries to the Ganga River. *Environmental Earth Sciences*, *77*(8), 313. https://doi.org/10.1007/s12665-018-7490-7

Bird, M. I., Robinson, R. A. J., Oo, N. W., Aye, M. M., Lu, X. X., Higgitt, D. L., et al. (2008). A preliminary estimate of organic carbon transport by the Ayeyarwady (Irrawaddy) and Thanlwin (Salween) Rivers of Myanmar. *Quaternary International*, *186*(1), 113–122. https://doi.org/10.1016/j.quaint.2007.08.003

Bonotto, D. M., & da Silveira, E. G. (2003). Preference ratios for mercury and other chemical elements in the Madeira River, Brazil. *Journal of South American Earth Sciences*, *15*(8), 911–923. https://doi.org/10.1016/S0895-9811(02)00144-X

Bouchez, J., Galy, V., Hilton, R. G., Gaillardet, J., Moreira-Turcq, P., Pérez, M. A., et al. (2014). Source, transport and fluxes of Amazon River particulate organic carbon: Insights from river sediment depth-profiles. *Geochimica et Cosmochimica Acta*, *133*, 280–298. https://doi.org/10.1016/j.gca.2014.02.032

Cameron, E. M., Hall, G. E., Veizer, J., & Krouse, H. R. (1995). Isotopic and elemental hydrogeochemistry of a major river system: Fraser River, British Columbia, Canada. *Chemical Geology*, *122*(1–4), 149–169. https://doi.org/10.1016/0009-2541(95)00007-9

Canfield, D. E. (1997). The geochemistry of river particulates from the continental USA: Major elements. *Geochimica et Cosmochimica Acta*, *61*(16), 3349–3365. https://doi.org/10.1016/S0016-7037(97)00172-5

Chapman, H., Bickle, M., Thaw, S. H., & Thiam, H. N. (2015). Chemical fluxes from time series sampling of the Irrawaddy and Salween Rivers, Myanmar. *Chemical Geology*, *401*, 15–27. https://doi.org/10.1016/j.chemgeo.2015.02.012

Christiansen, D. E. (2004). Riverbed elevations and water quality of the Missouri river at Sioux City, Iowa, 2002-03 (Report No. 2004–5079; Scientific Investigations Report). USGS Publications Warehouse. https://doi.org/10.3133/sir20045079

De Leeuw, J., Lamb, M. P., Parker, G., Moodie, A. J., Haught, D., Venditti, J. G., & Nittrouer, J. A. (2020). Entrainment and suspension of sand and gravel. *Earth Surface Dynamics*, *8*(2), 485–504. https://doi.org/10.5194/esurf-8-485-2020

Ding, T., Gao, J., Tian, S., Wang, H., Li, L. I., Wang, C., et al. (2016). Chemical and isotopic characters of the water and suspended particulate materials in the Yellow River and their geological and environmental implications. *Acta Geologica Sinica-English Edition*, *90*(1), 285–351. https://doi.org/10.1111/1755-6724.12658

Dosseto, A., Bourdon, B., Gaillardet, J., Allègre, C. J., & Filizola, N. (2006). Time scale and conditions of weathering under tropical climate: Study of the Amazon basin with U-series. *Geochimica et Cosmochimica Acta*, *70*(1), 71–89. https://doi.org/10.1016/j.gca.2005.06.033

Dosseto, A., Bourdon, B., Gaillardet, J., Maurice-Bourgoin, L., & Allègre, C. J. (2006). Weathering and transport of sediments in the Bolivian Andes: Time constraints from uranium-series isotopes. *Earth and Planetary Science Letters*, *248*(3–4), 759–771. https://doi.org/10.1016/j.epsl.2006.06.027

Elbaz-Poulichet, F., Seyler, P., Maurice-Bourgoin, L., Guyot, J.-L., & Dupuy, C. (1999). Trace element geochemistry in the upper Amazon drainage basin (Bolivia). *Chemical Geology*, *157*(3–4), 319–334. https://doi.org/10.1016/S0009-2541(99)00015-7

English, N. B., Quade, J., DeCelles, P. G., & Garzione, C. N. (2000). Geologic control of Sr and major element chemistry in Himalayan Rivers, Nepal. *Geochimica et Cosmochimica Acta*, *64*(15), 2549–2566. https://doi.org/10.1016/S0016-7037(00)00379-3

Friedman, J., Hastie, T., & Tibshirani, R. (2010). Regularization paths for generalized linear models via coordinate descent. *Journal of Statistical Software*, *33*(1), 1. https://doi.org/10.18637/jss.v033.i01

Galy, A., & France-Lanord, C. (1999). Weathering processes in the Ganges–Brahmaputra basin and the riverine alkalinity budget. *Chemical Geology*, *159*(1–4), 31–60. https://doi.org/10.1016/S0009-2541(99)00033-9

Garzanti, E., Wang, J.-G., Vezzoli, G., & Limonta, M. (2016). Tracing provenance and sediment fluxes in the Irrawaddy River basin (Myanmar). *Chemical Geology*, *440*, 73–90. https://doi.org/10.1016/j.chemgeo.2016.06.010

Guyot, J.-L., Jouanneau, J.-M., Quintanilla, J., & Wasson, J.-G. (1993). Dissolved and suspended sediment loads exported from the Andes by the Beni river (Bolivian Amazonia), during a Flood. *Geodinamica Acta*, *6*(4), 233–241. https://doi.org/10.1080/09853111.1993.11105251

Hedges, J. I., Mayorga, E., Tsamakis, E., McClain, M. E., Aufdenkampe, A., Quay, P., et al. (2000). Organic matter in Bolivian tributaries of the Amazon River: A comparison to the lower mainstream. *Limnology & Oceanography*, *45*(7), 1449–1466. https://doi.org/10.4319/lo.2000.45.7.1449

Hossain, H. Z., Kawahata, H., Roser, B. P., Sampei, Y., Manaka, T., & Otani, S. (2017). Geochemical characteristics of modern river sediments in Myanmar and Thailand: Implications for provenance and weathering. *Geochemistry*, *77*(3), 443–458. https://doi.org/10.1016/j.chemer.2017.07.005

Hu, B., Li, J., Bi, N., Wang, H., Wei, H., Zhao, J., et al. (2015). Effect of human-controlled hydrological regime on the source, transport, and flux of particulate organic carbon from the lower Huanghe (Yellow River). *Earth Surface Processes and Landforms*, *40*(8), 1029–1042. https://doi.org/10.1002/esp.3702

Huang, W. W., Jing, Z., & Zhou, Z. H. (1992). Particulate element inventory of the Huanghe (Yellow River): A large, high-turbidity river. *Geochimica et Cosmochimica Acta*, *56*(10), 3669–3680. https://doi.org/10.1016/0016-7037(92)90160-K

Huang, X., Sillanpää, M., Gjessing, E. T., & Vogt, R. D. (2009). Water quality in the Tibetan Plateau: Major ions and trace elements in the headwaters of four major Asian rivers. *The Science of the Total Environment*, *407*(24), 6242–6254. https://doi.org/10.1016/j.scitotenv.2009.09.001

Kelly, V., Hooper, R., Aulenbach, B., & Janet, M. (2001). Concentrations and annual fluxes for selected water-quality constituents from the USGS national stream quality accouting network (NASQAN), 1996-2000 (Report No. 01–4255; Water-Resources Investigations Report). United States Geological Survey.

Kleeschulte, M. J. (1993). Water-quality data for the Missouri River and Missouri River alluvium near Weldon Spring, St. Charles County, Missouri; 1991-92. In Open-File Report (No. 93–109). https://doi.org/10.3133/ofr93109

Lee, C. (2020). Nutrient and pesticide data collected from the USGS National Water Quality Network and previous networks, 1963-2019. [Data set]. U.S. Geological Survey. https://doi.org/10.5066/P9AEWTB9

Leenheer, J. A., Barber, L. B., Rostad, C. E., & Noyes, T. I. (1995). Data on natural organic substances in dissolved, colloidal, suspended-silt and -clay, and bed-sediment phases in the Mississippi River and some of its tributaries, 1991-92. (Report No. 94–4191; Water-Resources Investigations Report). USGS Publications Warehouse. https://doi.org/10.3133/wri944191

Li, J.-Y., & Zhang, J. (2003). Chemical Weathering Processes and Atmospheric CO2 Consumption in the Yellow River Drainage Basin. *Marine Geology & Quaternary Geology*, *23*(2), 43–49.

Malcolm, R. L., & Durum, W. H. (1976). *Organic carbon and nitrogen concentrations and annual organic carbon load of six selected rivers of the United States*. (Report No. 1817F; Water Supply Paper). USGS Publications Warehouse. https://doi.org/10.3133/wsp1817F

Manaka, T., Otani, S., Inamura, A., Suzuki, A., Aung, T., Roachanakanan, R., et al. (2015). Chemical weathering and long-term CO_2 consumption in the Ayeyarwady and Mekong river basins in the Himalayas. *Journal of Geophysical Research: Biogeosciences*, *120*(6), 1165–1175. https://doi.org/10.1002/2015JG002932

Piper, D. Z., Ludington, S., Duval, J. S., & Taylor, H. E. (2006). Geochemistry of bed and suspended sediment in the Mississippi river system: Provenance versus weathering and winnowing. *The Science of the Total Environment*, *362*(1–3), 179–204. https://doi.org/10.1016/j.scitotenv.2005.05.041

Qu, Y., Jin, Z., Wang, J., Wang, Y., Xiao, J., Gou, L.-F., et al. (2020). The sources and seasonal fluxes of particulate organic carbon in the Yellow River. *Earth Surface Processes and Landforms*, *45*(9), 2004–2019. https://doi.org/10.1002/esp.4861

Ran, L., Lu, X. X., Sun, H., Han, J., Li, R., & Zhang, J. (2013). Spatial and seasonal variability of organic carbon transport in the Yellow River, China. *Journal of Hydrology*, *498*, 76–88. https://doi.org/10.1016/j.jhydrol.2013.06.018

Richey, J. E., Victoria, R. L., Hedges, J. I., Dunne, T., Martinelli, L. A., Mertes, L., & Adams, J. (2008). Pre-LBA carbon in the Amazon River experiment (CAMREX) data. *ORNL DAAC*. https://doi.org/10.3334/ORNLDAAC/904

Sarin, M. M., Krishnaswami, S., Dilli, K., Somayajulu, B. L. K., & Moore, W. S. (1989). Major ion chemistry of the Ganga-Brahmaputra river system: Weathering processes and fluxes to the Bay of Bengal. *Geochimica et Cosmochimica Acta*, *53*(5), 997–1009. https://doi.org/10.1016/0016-7037(89)90205-6

Seyler, P. T., & Boaventura, G. R. (2003). Distribution and partition of trace metals in the Amazon basin. *Hydrological Processes*, *17*(7), 1345–1361. https://doi.org/10.1002/hyp.1288

SO-HYBAM. (n.d.). SO-HYBAM: Amazon basin water resources observation service. Retrieved from https://hybam.obs-mip.fr/

Spence, J., & Telmer, K. (2005). The role of sulfur in chemical weathering and atmospheric CO_2 fluxes: Evidence from major ions, δ13CDIC, and δ34SSO4 in rivers of the Canadian Cordillera. *Geochimica et Cosmochimica Acta*, *69*(23), 5441–5458. https://doi.org/10.1016/j.gca.2005.07.011

Stallard, R. F. (1980). Major element geochemistry of the Amazon River system [Doctoral thesis, Massachusetts Institute of Technology]. Retrieved from http://hdl.handle.net/1721.1/58120

Su, X., Wu, X., Lin, X., Liao, Z., & Wang, J. (2006). Main chemical components of the Yellow River water and downstream variations of δ13C. *Yellow River Water Resources*, 29–31.

Tipper, E. T., Stevenson, E. I., Alcock, V., Knight, A. C., Baronas, J. J., Hilton, R. G., et al. (2021). Global silicate weathering flux overestimated because of sediment–water cation exchange. *Proceedings of the National Academy of Sciences*, *118*(1). https://doi.org/10.1073/pnas.2016430118

Van Rijn, L. C. (1984). Sediment transport, Part II: Suspended load transport. *Journal of Hydraulic Engineering*, *110*(11), 1613–1641. https://doi.org/10.1061/(ASCE)0733-9429(1984)110

Voss, B. M. (2014). Spatial and temporal dynamics of biogeochemical processes in the Fraser river, Canada: A coupled organic-inorganic perspective. Retrieved from http://hdl.handle.net/1721.1/95521

Wang, B., Li, X., Yuan, H., Zhou, H., & Zhao, Y. (2009). Geochemistry of the main ions and Sr isotopic composition in the lower reach of the Yellow River, North China. *Environmental Chemistry*, *28*, 876–882.

Wang, X., Ma, H., Li, R., Song, Z., & Wu, J. (2012). Seasonal fluxes and source variation of organic carbon transported by two major Chinese Rivers: The Yellow River and Changjiang (Yangtze) River. *Global Biogeochemical Cycles*, *26*(2). https://doi.org/10.1029/2011GB004130

Yu, M., Eglinton, T. I., Haghipour, N., Montluçon, D. B., Wacker, L., Hou, P., et al. (2019). Impacts of natural and human-induced hydrological variability on particulate organic carbon dynamics in the Yellow River. *Environmental Science & Technology*, *53*(3), 1119–1129. https://doi.org/10.1021/acs.est.8b04705

Zhang, L.-J., & Wen, Z.-C. (2009). Discussion on Silicate Weathering in the Huanghe Drainage Basin. *Periodical of Ocean University of China*, *39*(5), 988–994.

Zhang, J., Huang, W. W., Letolle, R., & Jusserand, C. (1995). Major element chemistry of the Huanghe (Yellow River), China-weathering processes and chemical fluxes. *Journal of Hydrology*, *168*(1–4), 173–203. https://doi.org/10.1016/0022-1694(94)02635-O

Zhang, Q., Jin, Z., Zhang, F., & Xiao, J. (2015). Seasonal variation in river water chemistry of the middle reaches of the Yellow River and its controlling factors. *Journal of Geochemical Exploration*, *156*, 101–113. https://doi.org/10.1016/j.gexplo.2015.05.008